

Protocol for generating an arbitrary quantum state of the magnetization in cavity magnonics

Sanchar Sharma

Max Planck Institute for the Science of Light, 91058 Erlangen, Germany

Victor A. S. V. Bittencourt

Max Planck Institute for the Science of Light, 91058 Erlangen, Germany

Silvia Viola Kusminskiy

Institute for Theoretical Solid State Physics, RWTH Aachen University, 52074 Aachen, Germany

Max Planck Institute for the Science of Light, 91058 Erlangen, Germany

Abstract. We propose and numerically evaluate a protocol to generate an arbitrary quantum state of the magnetization in a magnet. The protocol involves repeatedly exciting a frequency-tunable superconducting transmon and transferring the excitations to the magnet via a microwave cavity. To avoid decay, the protocol must be much shorter than magnon lifetime. Speeding up the protocol by simply shortening the pulses leads to non-resonant leakage of excitations to higher levels of the transmon accompanied by higher decoherence. We discuss how to correct for such leakages by applying counter pulses to de-excite these higher levels. In our protocol, states with a maximum magnon occupation of up to ~ 9 and average magnon number up to ~ 4 can be generated with fidelity > 0.75 .

Magnets have found commercial applications in magnetic field sensing and storing of information, and are a promising building block for long-range information transfer [1, 2] and low-power logic devices [3]. Recently, there has been an interest in bringing such applications into the quantum domain, known as ‘quantum magnonics’ [4, 5, 6, 7]. This is partly fuelled by the extremely low magnetic dissipation found in the ferrimagnetic insulator Yttrium Iron Garnet (YIG) [8], along with evidence for macroscopic (mm-long) coherence lengths [9, 10]. In the limit of small deviations of spins from their equilibrium value, the collective excitations of a magnet can be modelled as a set of harmonic oscillators called magnons with a lifetime characterized by the Gilbert damping constant of the material that is particularly low for YIG [8]. Magnons can be probed via their interaction with microwaves (MWs) [11, 12, 13] or optical light [14, 15, 16, 17]. This interaction can be enhanced by employing an electromagnetic cavity to confine the photons, whose decay rate is given by the quality factor of the cavity. The strong coupling regime between cavity MW photons and magnons, where information can be coherently exchanged between the two excitations at rates > 10 MHz much faster than each of their decay rates < 1 MHz, can be routinely achieved in experiments. The strong coupling regime in the optical domain is notoriously more difficult to achieve, however there are promising developments in this direction [18, 19, 20, 21, 22, 23].

A quantum platform involving magnets requires generation, manipulation, and detection of non-classical states of the magnetization. Possible applications in the quantum regime include magnon-based quantum transducers between light and MWs, as well as transduction involving other degrees of freedom such as phonons [24, 25] and electrons [26, 27, 28]. Furthermore, non-classical magnetization states can be useful in magnetic field sensing reaching the Heisenberg limit [29]. While single-magnon detection has been demonstrated [30, 31, 32] by exploiting the coupling of magnets to superconducting circuits mediated by MW cavities [4, 33, 34, 35], experiments so far have probed coherent or thermal magnon states whereas “true” non-classical states (defined e.g. by a Wigner function with negative regions) remain to be realized. Theoretical proposals in this direction include the generation of cat states of the magnetization using MW cavity photons, [36] and the generation of single magnon Fock states [37] and cat states [38] via optical means. In thin films, the generation of entangled pairs of traveling magnons was proposed [39]. All of these proposals are probabilistic for the state generation (except for the last) and are specialized to their respective target states, while there is no known method to deterministically generate an arbitrary magnon state.

In this manuscript we fill in this gap by proposing a protocol to this end, tailored for magnets coupled to a superconducting transmon via a MW cavity, as depicted in Fig. 1. Our method is based on the protocol proposed in Ref. [40], which shows that the deterministic generation of an arbitrary quantum state of a harmonic oscillator can be accomplished by coupling the oscillator to a qubit. A superconducting transmon is a weakly anharmonic oscillator whose first two levels can be treated as a qubit. We show how the protocol of Ref. [40] can be modified to take into account the anharmonicity of the superconducting transmon, in order to generate arbitrary quantum magnon states

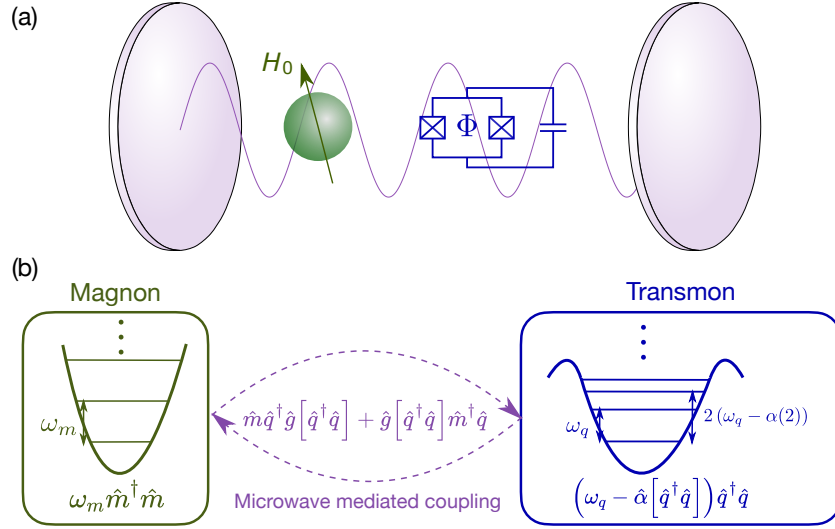


Figure 1. (a) The setup consists of a MW cavity loaded with a magnet and a superconducting transmon. The frequency of the Kittel mode can be tuned by an external magnetic field, while that of the transmon by using an input flux Φ . (b) Model of the system as a harmonic oscillator (magnons) coupled to an anharmonic oscillator (transmon). The coupling rate between magnon and transmon via the MWs depends on the transmon occupation. All the terms in the figure are defined in Sec. 1.

with high fidelity.

The paper is organized as follows. We discuss the system and effective Hamiltonian in Sec. 1. In Sec. 2 we approximate the superconducting transmon by a two-level system and review the protocol from Ref. [40] for the cavity magnonic system. In Sec. 3 we discuss how to correct for errors due to deviations from the two-level approximation, in particular due to interferences from higher energy levels present in the transmon. In Sec. 4, we discuss the fidelity of state generation for paradigmatic examples of non-classical states. We discuss possible improvements to our protocol that can increase the fidelity of generation further in Sec. 5. We review the main findings qualitatively in Sec. 6.

1. System

The hybrid system we considered is depicted in Fig. 1: inside a MW cavity, magnons can couple to a superconducting transmon [4, 33]. The effective coupling Hamiltonian can be obtained by tracing out the MW field, as we review in this section.

When the magnet is much smaller than the wavelength of the MWs (\sim cm), only the total magnetization \mathbf{M} couples to the MWs, so we need to consider only the uniform magnon mode known as the Kittel mode. It can be quantized via a Holstein-Primakoff transformation [41, 42] (see Appendix A for details) that, in the limit of $M_{x,y} \ll M_z$, reduces to

$$M_x - iM_y \rightarrow 2\mathcal{M}_{\text{ZPF}}\hat{M}, \quad M_z \rightarrow M_s - \frac{2\mathcal{M}_{\text{ZPF}}^2}{M_s}\hat{M}^\dagger\hat{M}. \quad (1)$$

where \hat{M} is the magnon annihilation operator satisfying the bosonic commutation relations $[\hat{M}, \hat{M}^\dagger] = 1$, M_s is the saturation magnetization, and the zero-point fluctuations of the magnetization are given by

$$\mathcal{M}_{\text{ZPF}} = \sqrt{\frac{\gamma \hbar M_s}{2V_m}}, \quad (2)$$

with $\gamma > 0$ being the absolute gyromagnetic ratio and V_m being the volume of the magnet. Assuming a spherical magnet and an external magnetic field H_{app} , the Hamiltonian becomes $\hat{H}_m = \hbar \Omega_m \hat{M}^\dagger \hat{M}$ with $\Omega_m = \gamma \mu_0 H_{\text{app}}$ (see Appendix A) which can be tuned to be in the range of $\sim 2\pi \times 5\text{-}10$ GHz. For a YIG sample with volume $V_m > 1 \mu\text{m}^3$, $M_s = 140 \text{ kA m}^{-1}$, and $\gamma = 2\pi \times 28 \text{ GHz T}^{-1}$, we have $\mathcal{M}_{\text{ZPF}}/M_s < 8 \times 10^{-6}$, implying that the deviations from the ground state are small.

A flux-tunable transmon consists of two Josephson junctions in parallel with Josephson energy $E_{J1, J2}$ respectively, forming a SQUID loop along with a capacitor with capacitance C also in parallel [43, 44, 45, 46]. When the charging energy $E_C = e^2/2C$ is such that $E_C \ll E_{J1, J2}$, the energy levels of the circuit resemble that of a weakly anharmonic oscillator,

$$E_n \approx \hbar \left(\Omega_q - \frac{A}{2}(n-1) \right) n, \quad (3)$$

where $A = E_C/4$ and $\Omega_q = \sqrt{E_C E_{J, \text{eff}}}$ with the effective Josephson energy $E_{J, \text{eff}}$ being

$$E_{J, \text{eff}}(\Phi) = \sqrt{(E_{J1} + E_{J2})^2 \cos^2 \frac{\pi \Phi}{\Phi_0} + (E_{J1} - E_{J2})^2 \sin^2 \frac{\pi \Phi}{\Phi_0}}. \quad (4)$$

Here Φ is the flux inside the SQUID loop and $\Phi_0 = h/2e$ is the superconducting flux quantum. Such a set of energy levels can be labelled using an annihilation operator \hat{Q} and its corresponding number operator $\hat{Q}^\dagger \hat{Q}$. The number of quanta exchanged between the two Josephson junctions is given by

$$\hat{N}_{\text{sc}} = \left(\frac{E_{J, \text{eff}}}{2E_C} \right)^{1/4} \frac{\hat{Q} - \hat{Q}^\dagger}{\sqrt{2i}}. \quad (5)$$

The Hamiltonian becomes

$$\hat{H}_{\text{tr}} = \hbar \left[\Omega_q - \frac{\hbar A}{2} (\hat{Q}^\dagger \hat{Q} - 1) \right] \hat{Q}^\dagger \hat{Q}. \quad (6)$$

The frequency Ω_q can be tuned dynamically via the external flux in SQUID Φ , to be in a typical range of $2\pi \times 5\text{-}20$ GHz. Tuning via Φ can be achieved at a fast timescale $\ll 10$ ns [47, 48], but it comes at the cost of increased decoherence proportional to the allowed tunability $|E_{J1} - E_{J2}|$, as a higher tunability implies larger susceptibility to flux noises [49, 45]. For our case, we assume that Ω_q is tunable within a range of $\sim 2\pi \times 1$ GHz.

We assume that the magnet and the transmon are both placed inside a MW cavity which can be modelled as a set of harmonic modes with frequencies $\Omega_{a,r}$ and annihilation operator \hat{A}_r . The details of the modes depend on the shape and size of the cavity. The Hamiltonian for the unloaded cavity is $\hat{H}_{\text{mw}} = \sum_r \hbar \Omega_{a,r} \hat{A}_r^\dagger \hat{A}_r$. Its coupling to both the

magnet and the transmon corresponds to exchange of quanta and can be modelled as [see Appendix A]

$$\frac{\hat{H}_{\text{int}}}{\hbar} = \sum_r \left(G_{m,r} \hat{M}^\dagger \hat{A}_r + G_{m,r}^* \hat{M} \hat{A}_r^\dagger + G_{q,r} \hat{Q}^\dagger \hat{A}_r + G_{q,r}^* \hat{Q} \hat{A}_r^\dagger \right), \quad (7)$$

where the coupling $G_{m,r} \propto |\mathbf{B}(\mathbf{r}_{\text{magnet}})|$ with $\mathbf{B}(\mathbf{r}_{\text{magnet}})$ the magnetic field at the location of the magnet, and $G_{q,r} \propto |\mathbf{E}(\mathbf{r}_{\text{transmon}})|$ where $\mathbf{E}(\mathbf{r}_{\text{transmon}})$ is the electric field at the location of the transmon. If for all r modes, $\Omega_{a,r} - \Omega_m > G_{m,r}$ and $\Omega_{a,r} - \Omega_q > G_{q,r}$, we can define cavity-dressed magnon and transmon modes with annihilation operators \hat{m} and \hat{q} respectively. Up to quadratic order in the couplings [4],

$$\frac{\hat{H}}{\hbar} = \omega_m \hat{m}^\dagger \hat{m} + \left(\omega_q - \hat{\alpha} [\hat{q}^\dagger \hat{q}] \right) \hat{q}^\dagger \hat{q} + \hat{m} \hat{q}^\dagger \hat{g} [\hat{q}^\dagger \hat{q}] + \hat{g} [\hat{q}^\dagger \hat{q}] \hat{m}^\dagger \hat{q}. \quad (8)$$

Details about this Hamiltonian are provided in Appendix A, while here we list down the features relevant for the rest of the article. The renormalized magnon's frequency ω_m and transmon's frequency ω_q stay close to their bare values Ω_m and Ω_q respectively. A schematic representation of each term of the Hamiltonian is shown in Fig. 1.

The function $\hat{\alpha}$ gives the anharmonicity of the transmon and \hat{g} gives the magnon-transmon coupling. Below, we use the same characters $\alpha(n) = \langle n | \hat{\alpha} | n \rangle$ and $g(n) = \langle n | \hat{g} | n \rangle$ for the values of anharmonicity and coupling. Typically $\alpha(2) \sim 2\pi \times 150\text{-}300$ MHz increasing with n and the coupling g can achieve $\sim 2\pi \times 20\text{-}30$ MHz depending on the system parameters as discussed in Appendix A.

Restricting the analysis to only the first two levels of the transmon, we get the Jaynes-Cummings Hamiltonian

$$\frac{\hat{H}^{(2)}}{\hbar} = \omega_m \hat{m}^\dagger \hat{m} + \omega_q |e\rangle \langle e| + g \left(\hat{m} \hat{\sigma}_+ + \hat{m}^\dagger \hat{\sigma}_- \right), \quad (9)$$

where $g \equiv g(0)$, $\{|g\rangle, |e\rangle\}$ are the first two excited states of the transmon, $\hat{\sigma}_+ = |g\rangle \langle e|$ and $\hat{\sigma}_- = |e\rangle \langle g|$. As mentioned before, the frequency ω_q is tunable. When $|\omega_q - \omega_m| \gg g$, the magnons and transmon are decoupled besides a negligible dispersive coupling, while at resonance, $\omega_q = \omega_m$, the two subsystems can exchange quanta.

2. Ideal State Generation

In this section we review the protocol to generate an arbitrary state of the magnetization via its coupling to a two-level system. This is discussed in [40] theoretically for a general harmonic oscillator. The protocol consists of: (1) exciting the qubit; (2) partially transferring the excitation to the oscillator and (3) repeating the process multiple times to construct the Fock-state superposition that describes the target state. In this setup, the transmon can be excited via a time-dependent drive, while the transmon and the magnons can be put in and out of resonance by tuning the magnon frequency (via an external magnetic field) or the transmon frequency (via an applied flux), effectively changing the coupling rate (see Fig. 2). The procedure was experimentally implemented to generate quantum states of MW photons coupled to a superconducting transmon [48].

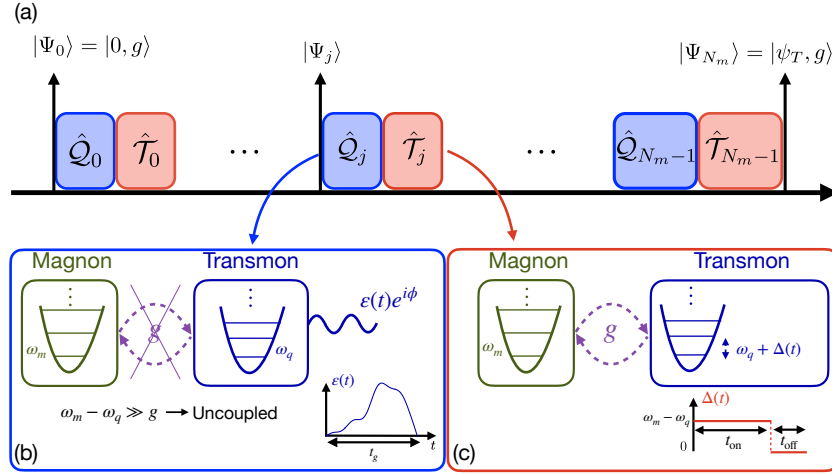


Figure 2. (a) Schematic representation of the protocol for generation of an arbitrary magnon state, starting from $|0, g\rangle$, i.e. both magnon and transmon being in ground state, ending in $|\psi_T, g\rangle$, i.e. the magnon being in a target state $|\psi_T\rangle$ and transmon in ground state. (b) The qubit gate is implemented via a time-dependent drive $\tilde{\varepsilon}(t) = \varepsilon(t)e^{i\phi}e^{-i\omega_q t}$, and (c) the quanta exchange is accomplished by tuning the transmon's frequency via the term $\Delta(t)$, see Eq. 12. The target superposition is constructed by choosing appropriate $\{\varepsilon(t), \phi\}$ and $\{t_{\text{on}}, t_{\text{off}}\}$ at each stage of the protocol.

If we start from the qubit's state $c_0 |e\rangle + c_1 |g\rangle$ while the magnon is in the ground state $|0\rangle$, switching the coupling on for a period $t = \pi/(2g)$ in the absence of dissipation evolves the state as

$$(c_0 |e\rangle + c_1 |g\rangle) |0\rangle \rightarrow |g\rangle (c_0 |0\rangle + c_1 |1\rangle), \quad (10)$$

where $|n\rangle$ is n -magnon state. Thus, we can create an arbitrary superposition of $|0\rangle$ and $|1\rangle$. If we repeat this process N times, we can, in principle, generate an arbitrary magnon state containing up to a maximum of N magnons. The protocol then consists of a series of operations in which first the transmon is excited, and then the qubit's frequency is changed to bring it in resonance with the magnons for a time of the order π/g .

To make the process concrete, consider the Hamiltonian restricted to the first two levels of the transmon $\hat{H}^{(2)}(t) = \hat{H}_s^{(2)} + \hat{H}_d^{(2)}(t)$, where the static part is

$$\frac{\hat{H}_s^{(2)}}{\hbar} = \omega_m \hat{m}^\dagger \hat{m} + \omega_q |e\rangle \langle e| + g (\hat{m} \hat{\sigma}_+ + \hat{m}^\dagger \hat{\sigma}_-), \quad (11)$$

and the dynamic part is

$$\frac{\hat{H}_d^{(2)}}{\hbar} = \Delta(t) |e\rangle \langle e| + \tilde{\varepsilon}(t) \hat{\sigma}_+ + \tilde{\varepsilon}^*(t) \hat{\sigma}_-, \quad (12)$$

Here and in what follows, the superscript (2) indicates the approximation of the transmon as a two-level system. In this expression, $\Delta(t)$ is the externally induced change in the transmon's frequency, and $\tilde{\varepsilon}(t)$ is the transmon drive amplitude. We

assume that the qubit and the magnons are far detuned, $|\omega_m - \omega_q| \gg g$, implying that magnons and qubit are decoupled at $\Delta = 0$.

A non-zero $\tilde{\varepsilon}$ can excite a qubit. We define the time evolution operator $\hat{Q}^{(2)}$ for $\Delta = 0$ and $\tilde{\varepsilon}(t) = \varepsilon(t)e^{-i\omega_q t + i\phi}$,

$$\hat{Q}^{(2)}(\theta, \phi) = \text{Texp} \left[-\frac{i}{\hbar} \int_0^{t_g} dt \left(\hat{H}_s^{(2)} - \hbar \varepsilon(t) e^{-i\omega_q t + i\phi} \hat{\sigma}_+ + \text{h.c.} \right) \right], \quad (13)$$

where t_g is a pre-determined gate time, $\varepsilon(t)$ is chosen satisfying $\int_0^{t_g} d\tau \varepsilon(\tau) = \theta$ and Texp is the time-ordered exponential. As derived in Appendix C,

$$\hat{Q}^{(2)}(\theta, \phi) = e^{-i\omega_m t_g \hat{m}^\dagger \hat{m} - i\omega_q t_g |e\rangle \langle e|} \left(\hat{I} \cos \theta + i \sin \theta \left(e^{i\phi} \hat{\sigma}_+ + e^{-i\phi} \hat{\sigma}_- \right) \right), \quad (14)$$

which applies a Bloch rotation of magnitude 2θ around the axis $(\cos \phi, -\sin \phi, 0)$. After the qubit is excited, we want to (partially) transfer the quanta to magnons. We then define the time evolution operator for a detuning $\Delta_0 = \omega_m - \omega_q$ and no qubit driving

$$\hat{\mathcal{T}}^{(2)}(t_{\text{on}}, t_{\text{off}}) = \exp \left[\frac{-i \hat{H}_s^{(2)} t_{\text{off}}}{\hbar} \right] \exp \left[-\frac{i}{\hbar} \left(\hat{H}_s^{(2)} + \Delta_0 |e\rangle \langle e| \right) t_{\text{on}} \right]. \quad (15)$$

An additional ‘off’ time, t_{off} , adjusts the relative phases in the wave-function ‡. As derived in Appendix B, $\hat{\mathcal{T}}^{(2)} = \hat{\mathcal{T}}_{\text{ph}}^{(2)} \hat{\mathcal{T}}_{\text{ex}}^{(2)}$ where the phases evolve as

$$\hat{\mathcal{T}}_{\text{ph}}^{(2)} = \exp \left(-i\omega_m (t_{\text{off}} + t_{\text{on}}) \hat{m}^\dagger \hat{m} - i(\omega_m t_{\text{on}} + \omega_q t_{\text{off}}) |e\rangle \langle e| \right), \quad (16)$$

and the quanta are exchanged via

$$\hat{\mathcal{T}}_{\text{ex}}^{(2)} = \cos \left(g t_{\text{on}} \sqrt{\hat{N}} \right) - \frac{i}{\sqrt{\hat{N}}} \sin \left(g t_{\text{on}} \sqrt{\hat{N}} \right) \left(\hat{m} \hat{\sigma}_+ + \hat{m}^\dagger \hat{\sigma}_- \right), \quad (17)$$

with the total number operator $\hat{N} = \hat{m}^\dagger \hat{m} + |e\rangle \langle e|$.

A given target state $|\psi_T\rangle$ containing a maximum of N_m magnons, can be systematically achieved by adding magnons one by one as described above. For that, we need a set of time evolution operators $\hat{Q}_j^{(2)} \equiv \hat{Q}^{(2)}(\theta_j, \phi_j)$ and $\hat{\mathcal{T}}_j^{(2)} \equiv \hat{\mathcal{T}}^{(2)}(t_{\text{on},j}, t_{\text{off},j})$ (see Fig. 2) such that

$$|\Psi_0\rangle = |0, g\rangle, \quad |\Psi_{j+1}\rangle = \hat{\mathcal{T}}_j^{(2)} \hat{Q}_j^{(2)} |\Psi_j\rangle, \quad |\Psi_{N_m}\rangle = |\psi_T, g\rangle, \quad (18)$$

and each $|\Psi_j\rangle$ has a maximum of j excitations. Explicitly, for $|\Psi_j\rangle = |\psi_j^e, e\rangle + |\psi_j^g, g\rangle$ there are a maximum of $(j-1)$ and j magnons in $|\psi_j^e\rangle$ and $|\psi_j^g\rangle$ respectively.

The coefficients $\{\theta_j, \phi_j, t_{\text{off},j}, t_{\text{on},j}\}$ are found by reversing the problem in order to systematically remove magnons one by one from $|\Psi_{N_m}\rangle$. Inductively, we assume that $|\Psi_{j+1}\rangle$ is found. Explicitly, we find $\{t_{\text{on},j}, t_{\text{off},j}\}$ to ensure $\langle j+1, g | \hat{\mathcal{T}}_j^{(2),\dagger} |\Psi_{j+1}\rangle = 0$ achieved via [see Appendix B]

$$\langle j+1, g | \Psi_{j+1}\rangle \cos \left(g t_{\text{on},j} \sqrt{j+1} \right) + i \langle j, e | \Psi_{j+1}\rangle \sin \left(g t_{\text{on},j} \sqrt{j+1} \right) e^{-i\Delta_0 t_{\text{off},j}} = 0. \quad (19)$$

Next, we find $\{\theta_j, \phi_j\}$ to ensure $\langle j, e | \hat{Q}_j^{(2),\dagger} \hat{\mathcal{T}}_j^{(2),\dagger} |\Psi_{j+1}\rangle = 0$ giving [see Appendix C]

$$\langle j, e | \hat{\mathcal{T}}_j^{(2),\dagger} |\Psi_{j+1}\rangle \cos \theta_j + i \langle j, g | \hat{\mathcal{T}}_j^{(2),\dagger} |\Psi_{j+1}\rangle \sin \theta_j e^{i\phi_j - i\omega_q t_g} = 0. \quad (20)$$

‡ In [40], the coupling was assumed to be a freely varying complex parameter, so the phases could be adjusted via the phase of g .

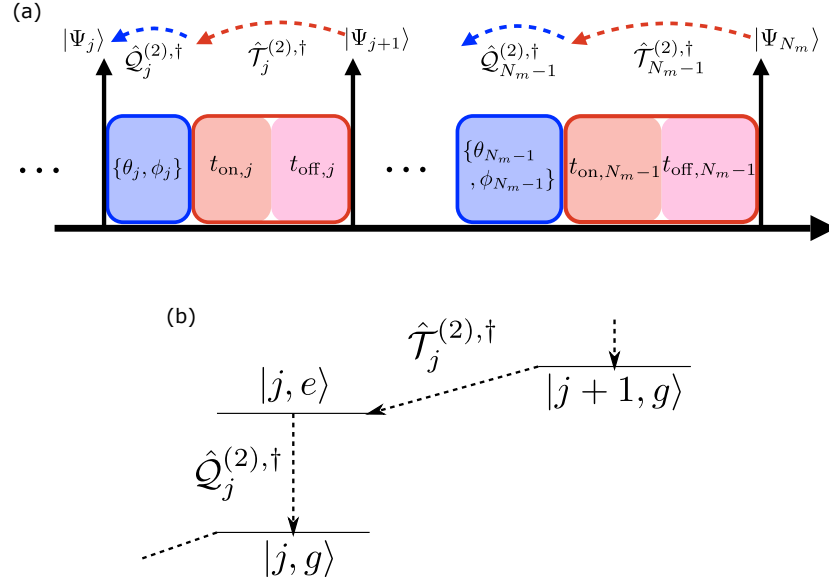


Figure 3. (a) The parameters are determined inductively from the last operation to the first. Starting from the target state $|\Psi_{N_m}\rangle = |\psi_T, g\rangle$, each application of $(\hat{T}_j^{(2)} \hat{Q}_j^{(2)})^\dagger$ removes one quanta from the magnon-transmon system. (b) $\hat{T}_j^{(2),\dagger}$ is chosen to ensure $\langle j+1, g | \hat{T}_j^{(2),\dagger} | \Psi_{j+1} \rangle = 0$ that can be interpreted as transferring amplitude from $|j+1, g\rangle$ to $|j, e\rangle$. Similarly, ensuring $\langle j, e | \hat{Q}_j^{(2),\dagger} \hat{T}_j^{(2),\dagger} | \Psi_{j+1} \rangle = 0$ can be interpreted as transferring the amplitude from $|j, e\rangle$ to $|j, g\rangle$.

Then, we find $|\Psi_j\rangle = (\hat{T}_j^{(2)} \hat{Q}_j^{(2)})^\dagger |\Psi_{j+1}\rangle$ and the induction continues until all quanta are removed. The procedure to inductively obtain the protocol's parameters is schematically shown in Fig. 3.

3. Realistic State Generation

The protocol discussed in the previous section is suitable to generate states with only a small number of excitations. States with higher number occupation require longer protocols and hence are spoiled by dissipation. The protocol duration can be decreased via two ways. Firstly, the gate time to excite the qubit can be decreased. Nevertheless, for a transmon qubit, a shorter gate time, $t_g \sim 1/\alpha(n)$ where α is the level-dependent anharmonicity [see below Eq. (8)], implies a broader frequency spectrum allowing for significant non-resonant transitions to higher transmon levels. Secondly, a stronger coupling between magnons and the transmon speeds up the excitation transfer step. However, a very strong coupling, $g(n)\sqrt{n} \sim \alpha(n)$ where g is the level-dependent magnon-transmon coupling [see below Eq. (8)], implies a leakage of magnon excitations into higher transmon states. Such interferences limit the protocol time and eventually the largest size of the harmonic oscillator state that can be created. In this section, we show that transitions to higher levels can be incorporated by adding extra pulses for

canceling out such transition amplitudes. The extra pulses are analogous to the ones used for correcting qubit gates [50, 51] and can significantly decrease the protocol time allowing for states containing a large magnon number.

For clarity in presentation, we consider the case of $g(n) \equiv g$ and

$$\alpha(n) \equiv \frac{\alpha}{2} (n - 1), \quad (21)$$

while the calculations for the general case are presented in Appendix B and Appendix C. The Hamiltonian, Eq. (8), becomes $\hat{H} = \hat{H}_s + \hat{H}_d(t)$, where the static part is

$$\frac{\hat{H}_s}{\hbar} = \omega_m \hat{m}^\dagger \hat{m} + \left(\omega_q - \frac{\alpha}{2} (\hat{q}^\dagger \hat{q} - 1) \right) \hat{q}^\dagger \hat{q} + g (\hat{m} \hat{q}^\dagger + \hat{m}^\dagger \hat{q}), \quad (22)$$

and the dynamic part is

$$\frac{\hat{H}_d(t)}{\hbar} = \Delta(t) \hat{q}^\dagger \hat{q} + \tilde{\varepsilon}(t) \hat{q}^\dagger + \tilde{\varepsilon}^*(t) \hat{q}. \quad (23)$$

For a target magnon state $|\psi\rangle$, we want to find a set of operations \hat{Q}_j and \hat{T}_j satisfying (see Fig. 2)

$$|\Psi_0\rangle = |0, 0\rangle, \quad |\tilde{\Psi}_j\rangle = \hat{Q}_j |\Psi_j\rangle, \quad |\Psi_{j+1}\rangle = \hat{T}_j |\tilde{\Psi}_j\rangle, \quad |\Psi_{N_m}\rangle = |\psi, 0\rangle, \quad (24)$$

where $|\psi_1, \psi_2\rangle$ refers to the magnon state $|\psi_1\rangle$ and transmon state $|\psi_2\rangle$. As before, starting from $|\Psi_{N_m}\rangle$, we inductively find $\{\hat{T}_j, \hat{Q}_j, |\Psi_j\rangle\}$ where the transfer operator ensures $\langle j+1, 0 | \hat{T}_j^\dagger | \Psi_{j+1} \rangle = 0$ (removing a magnon) and the gate operation ensures

$$\langle j+1-s, s | \hat{Q}_j^\dagger | \tilde{\Psi}_j \rangle = 0, \quad (25)$$

for $s \geq 1$ (removing transmon excitations).

3.1. Transfer of excitation

In Appendix B, we derive \hat{T}_j satisfying the condition $\langle j+1, 0 | \hat{T}_j^\dagger | \Psi_{j+1} \rangle = 0$, while we discuss the salient features of the derivation here. We start with the same ansatz as before [see Eq. (15)]

$$\hat{T}^{\text{ans}}(t_{\text{on}}, t_{\text{off}}) = \exp\left[\frac{-i\hat{H}_s t_{\text{off}}}{\hbar}\right] \exp\left[-\frac{i}{\hbar} (\hat{H}_s + \Delta_0 \hat{q}^\dagger \hat{q}) t_{\text{on}}\right], \quad (26)$$

except for the fact that the Hamiltonian includes all higher transmon levels. This ansatz can be simplified by noticing that the number of excitations $\hat{N} = \hat{m}^\dagger \hat{m} + \hat{q}^\dagger \hat{q}$ are conserved during the evolution, i.e. $[\hat{N}, \hat{T}^{\text{ans}}] = \hat{0}$. An expression for \hat{T}^{ans} restricted to the space of $\{|j+1-s, s\rangle\}_{s \geq 0}$ can be found by numerically diagonalizing the two Hamiltonians, \hat{H}_s and $\hat{H}_s + \Delta_0 \hat{q}^\dagger \hat{q}$. Finally, we get a condition on $\{t_{\text{on}}, t_{\text{off}}\}$ of the form

$$\sum_{pqr} e^{i\lambda_{\text{on}}^{(p)} t_{\text{on}}} e^{i\lambda_{\text{off}}^{(q)} t_{\text{off}}} a_{pq}^{(r)} \langle j+1-r, r | \Psi_{j+1} \rangle = 0, \quad (27)$$

where $\{\lambda_{\text{on}}^{(p)}, \lambda_{\text{off}}^{(q)}, a_{pq}^{(r)}\}$ can be found in terms of the eigenvectors and eigenvalues of the Hamiltonians [see Appendix B]. This equation can be numerically solved for $\{t_{\text{on}}, t_{\text{off}}\}$.

The above ansatz yields a solution in most cases, nevertheless, it can fail for some states, for example, when $|\Psi_{j+1}\rangle = |j+1, 0\rangle$. Intuitively, when the coupling is on, the excitation from $|j+1, 0\rangle$ transfers to all $|j+1-s, s\rangle$ but with different oscillation frequencies $\sim \sqrt{g^2 + \frac{\alpha^2 s^2 (s-1)^2}{4}}$. Unless these oscillation frequencies are commensurate, the amplitude of the wave-function in $|j+1, 0\rangle$ will stay non-zero.

In cases where this ansatz fails, we can apply a second operation,

$$\hat{\mathcal{T}}_j = \hat{\mathcal{T}}_j^{\text{ans}} \left(t_{\text{on},j}^{(2)}, t_{\text{off},j}^{(2)} \right) \hat{\mathcal{T}}_j^{\text{ans}} \left(t_{\text{on},j}^{(1)}, t_{\text{off},j}^{(1)} \right), \quad (28)$$

where we choose $\{t_{\text{on},j}^{(1)}, t_{\text{off},j}^{(1)}\}$ as the values found from a two-level approximation [see Eq. (20)], and $\{t_{\text{on},j}^{(2)}, t_{\text{off},j}^{(2)}\}$ are found by applying the above optimization to $\hat{\mathcal{T}}_j^{\text{ans},\dagger} \left(t_{\text{on},j}^{(1)}, t_{\text{off},j}^{(1)} \right) |\Psi_{j+1}\rangle$. In principle, this process can be continued until a solution is found. However, in our simulations, we never had to go beyond a second step.

3.2. Transmon gates

As noted before, the application of $\hat{\mathcal{Q}}_j$ ensures that $\hat{\mathcal{Q}}_j^\dagger |\tilde{\Psi}_j\rangle$ has no excitations above the level j . The results are derived in Appendix C and here, we discuss the salient features of the derivation. First, we want to apply a gate between transmon states $|0\rangle$ and $|1\rangle$, $\hat{\mathcal{Q}}_{01}^{\text{ideal}}(\theta_j^{01}, \phi_j^{01})$, to “transfer” the amplitude of $|j, 1\rangle$ to $|j, 0\rangle$, i.e. ensure $\langle j, 1 | \hat{\mathcal{Q}}_{01}^{\text{ideal},\dagger} |\tilde{\Psi}_j\rangle = 0$, where $\{\theta_j^{01}, \phi_j^{01}\}$ are given by

$$\langle j, 1 | \tilde{\Psi}_j \rangle \cos \theta_j^{01} + i \langle j, 0 | \tilde{\Psi}_j \rangle \sin \theta_j^{01} e^{i\phi_j^{01}} = 0, \quad (29)$$

which can be obtained using the same arguments as in the two-level approximation, see Eq. (20). To implement this with realistic signal, we use the ansatz

$$\hat{\mathcal{Q}}_{01}(t) = \text{Texp} \left[-\frac{i}{\hbar} \int_0^t dt \left(\hat{H}_s - \hbar \varepsilon(\tau) e^{-i\omega_q \tau + i\phi_{\text{app}}} \hat{q}^\dagger + \text{h.c.} \right) \right], \quad (30)$$

where $\{\varepsilon(t), \phi_{\text{app}}\}$ are to be determined. We can separate the phases by

$$\hat{\mathcal{Q}}_{01}(t) \approx \exp \left[-i \left(\omega_m \hat{m}^\dagger \hat{m} + \omega_q \hat{q}^\dagger \hat{q} \right) t \right] e^{i\phi_{\text{app}} \hat{q}^\dagger \hat{q}} \hat{\mathcal{U}}_{01}(t) e^{-i\phi_{\text{app}} \hat{q}^\dagger \hat{q}}, \quad (31)$$

where we ignore the interaction between magnons and photons (they are far off-resonant) and

$$\hat{\mathcal{U}}_{01}(t) = \text{Texp} \left[i \int_0^t d\tau \varepsilon(\tau) \left(\sum_{n=0}^{\infty} \sqrt{n+1} e^{-inA\tau} |n+1\rangle \langle n| + \text{h.c.} \right) \right]. \quad (32)$$

In the two-level approximation, we can choose any $\varepsilon^{(0)}(t)$ satisfying $\int_0^{t_g} d\tau \varepsilon^{(0)}(\tau) = \theta_j^{01}$ and $\phi_{\text{app}}^{(0)} = \phi_j^{01} - \omega_q t_g$. For concreteness, we choose

$$\varepsilon^{(0)}(t) = \frac{\pi \theta_j^{01}}{2t_g} \sin \left(\frac{\pi t}{t_g} \right), \quad (33)$$

where t_g is a pre-determined gate time. In the two-level approximation, the time-dependence is given by

$$\hat{\mathcal{U}}_{01}^{(0)}(t) = \text{Texp} \left[i \int_0^t d\tau \varepsilon^{(0)}(\tau) (|1\rangle \langle 0| + \text{h.c.}) \right]. \quad (34)$$

As the term in the exponential commutes with itself at all times, we can remove the time-ordering operator and simplify $\hat{\mathcal{U}}_{01}^{(0)}$ to,

$$\hat{\mathcal{U}}_{01}^{(0)}(t) = \cos \Theta(t) (|0\rangle \langle 0| + |1\rangle \langle 1|) + i \sin \Theta(t) (|1\rangle \langle 0| + |0\rangle \langle 1|) + \sum_{n=2}^{\infty} |n\rangle \langle n|, \quad (35)$$

where $\Theta(t) = \int_0^t \varepsilon^{(0)}(\tau) d\tau$.

However, a drive amplitude with a general form $\varepsilon(t)$ can induce transitions to higher transmon levels, e.g. transitions between $|j, 1\rangle$ and $|j, 2\rangle$. This is problematic as a significant transition amplitude $\langle j, 2 | \hat{\mathcal{Q}}_j^\dagger | \tilde{\Psi}_j \rangle$ implies excitation number $j+2$, while we want $\hat{\mathcal{Q}}_j^\dagger | \tilde{\Psi}_j \rangle$ to have no excitations above j . Thus, we consider $\varepsilon(t) = \varepsilon^{(0)}(t) + \varepsilon^{(1)}(t)$, where $\varepsilon^{(1)}(t)$ are higher frequency components that cancel out higher order transitions, making $\hat{\mathcal{U}}_{01} \approx \hat{\mathcal{U}}_{01}^{(0)}$.

The error in the transmon gate is given by

$$\hat{\mathcal{U}}_{\text{err}}(t) = \hat{\mathcal{U}}_{01}^{(0),\dagger}(t) \hat{\mathcal{U}}_{01}(t) = \text{Texp} \left[i \int_0^t d\tau \delta \hat{h}(\tau) - h.c. \right], \quad (36)$$

where

$$\delta \hat{h}(\tau) = \hat{\mathcal{U}}_{01}^{(0),\dagger}(\tau) \left(\varepsilon(\tau) \sum_{n=0}^{\infty} \sqrt{n+1} e^{-inA\tau} |n+1\rangle \langle n| - \varepsilon^{(0)}(\tau) |1\rangle \langle 0| \right) \hat{\mathcal{U}}_{01}^{(0)}(\tau). \quad (37)$$

$\hat{\mathcal{U}}_{\text{err}}$ cannot be found analytically. To linear order in the perturbation, we ignore the corrections due to non-commutativity, and impose

$$\int_0^{t_g} d\tau \delta \hat{h}(\tau) = \hat{0}. \quad (38)$$

This in turn implies the following set of equations that the drive amplitude $\varepsilon(t)$ must satisfy

$$\int_0^{t_g} (\varepsilon(\tau) - \varepsilon^{(0)}(\tau)) d\tau = 0, \quad (39)$$

$$\int_0^{t_g} \varepsilon(\tau) e^{iA\tau \pm i\Theta(t)} d\tau = 0, \quad (40)$$

$$n \geq 2 : \int_0^{t_g} \varepsilon(\tau) e^{in\tau} d\tau = 0. \quad (41)$$

The first condition is a no-bias condition ensuring that $\int_0^{t_g} \varepsilon(\tau) d\tau = \theta_j^{01}$. The second condition, with $\Theta(t) = \int_0^t d\tau \varepsilon^{(0)}(\tau)$ ensures that the transitions $|1\rangle \leftrightarrow |2\rangle$ cancel out at the end of the gate. Similarly, the transitions $|n\rangle \leftrightarrow |n+1\rangle$ are cancelled by the third condition. In our simulations, we find that for typical parameters, the population beyond level 2 is negligible, so we can ignore the conditions for $n \geq 3$.

The above conditions leave sufficient freedom in choosing $\varepsilon(t)$. In what follows, we choose $t_g = 3\pi/\alpha$ and

$$\varepsilon(t) = \sum_{\mu=0}^4 \varepsilon_\mu \sin \left(\frac{(2\mu+1)\pi t}{t_g} \right), \quad (42)$$

where the parameters ε_μ are governed by an underdetermined set of linear equations that can be found from the above conditions [shown explicitly in Appendix C]. Given $\varepsilon(t)$, we can find ϕ_{app} by minimizing $|\langle j, 1 | \hat{\mathcal{Q}}_{01}^\dagger | \tilde{\Psi}_j \rangle|$ as discussed in Appendix C.3.

We point out that although we choose a linear approximation, the corrections are not always small. However, in our simulations we find that the error matrix $\hat{\mathcal{U}}_{\text{err}}$ is dominated by extraneous phases for all transmon levels. One might think that these can be removed by adding higher order corrections, however, we observed that such higher order corrections typically shifts the errors from $|2\rangle$ to $|n \geq 3\rangle$ instead of removing them §. Thus, we account for these extra phases by modifying the next steps of the induction.

If $|\langle j-1, 2 | \hat{\mathcal{Q}}_{01}^\dagger | \tilde{\Psi}_j \rangle|$ is significant (we take the threshold as 0.1 in our simulations), a second gate between $|1\rangle$ and $|2\rangle$, say $\hat{\mathcal{Q}}_{12}^{\text{ideal}}(\theta_j^{12}, \phi_j^{12})$, can be applied to ensure that $\langle j-1, 2 | \hat{\mathcal{Q}}_{12}^{\text{ideal}, \dagger} \hat{\mathcal{Q}}_{01}^\dagger | \tilde{\Psi}_j \rangle = 0$, with

$$\langle j, 1 | \hat{\mathcal{Q}}_{01}^\dagger | \tilde{\Psi}_j \rangle \cos \theta_j^{12} + i \langle j, 0 | \hat{\mathcal{Q}}_{01}^\dagger | \tilde{\Psi}_j \rangle \sin \theta_j^{12} e^{i\phi_j^{12}} = 0. \quad (43)$$

Essentially, the same arguments presented above hold for the gate $\hat{\mathcal{Q}}_{12}$ defined by

$$\hat{\mathcal{Q}}_{12}[\varepsilon(t), \phi_{\text{app}}] = \text{Texp} \left[-\frac{i}{\hbar} \int_0^{t_g} dt \left(\hat{H}_s - \frac{\hbar \varepsilon(t)}{\sqrt{2}} e^{-i(\omega_q - A)t + i\phi_{\text{app}}} \hat{q}^\dagger + \text{h.c.} \right) \right], \quad (44)$$

where we can choose

$$\varepsilon^{(0)}(t) = \frac{\pi \theta_j^{12}}{2t_g} \sin \left(\frac{\pi t}{t_g} \right) \quad (45)$$

and $\varepsilon(t)$ satisfying the same conditions as before.

The levels $|n \geq 3\rangle$ are found to be approximately unoccupied, so we do not need to apply more gates.

4. Results

To evaluate the above algorithm, we numerically solve the time evolution that implements the protocol for the density matrix, using QuTiP [52, 53], satisfying

$$\frac{d\hat{\rho}}{dt} = -\frac{i}{\hbar} [\hat{H}_s + \hat{H}_d(t), \hat{\rho}(t)] + \sum_n \frac{1}{2} [2\hat{C}_n \hat{\rho}(t) \hat{C}_n^\dagger - \hat{\rho}(t) \hat{C}_n^\dagger \hat{C}_n - \hat{C}_n^\dagger \hat{C}_n \hat{\rho}(t)]. \quad (46)$$

For dissipation, we take the Lindblad operators pertaining to magnon decay $\hat{C}_1 = \sqrt{\kappa_m} \hat{m}$, transmon decay $\hat{C}_2 = \sqrt{\kappa_q} \hat{q}$ and transmon dephasing $\hat{C}_3 = \sqrt{\gamma_q} \hat{q}^\dagger \hat{q}$. We did not include magnon dephasing as it has not yet been experimentally observed, although there are theoretical reasons for pure dephasing of magnons [54]. We choose typical parameters $\omega_m = 2\pi \times 6$ GHz, $\omega_q = 2\pi \times 5$ GHz, $\kappa_m = 10^{-4} \omega_m$, $\kappa_q = \gamma_q = 10^{-4} \omega_q$, $A = 2\pi \times 300$ MHz, and coupling $g = 2\pi \times 25$ MHz. For a given target state $|\psi_T\rangle$, the algorithm described in the previous sections gives the signals $\Delta[\psi_T](t)$ and $\tilde{\varepsilon}[\psi_T](t)$, along with the protocol time $T_{\text{tot}}[\psi_T]$. Starting from the ground state, $|0, 0\rangle$, we numerically solve the above Lindblad equation with the given signals, Δ and $\tilde{\varepsilon}$, and find the reduced density matrix for the magnon, $\hat{\rho}_{\text{mag}}[\psi_T] = \text{Tr}_{\hat{q}}[\hat{\rho}(t[\psi_T])]$:

$$|\psi_T\rangle \xrightarrow{\text{protocol}} \{\Delta(t), \tilde{\varepsilon}(t)\} \xrightarrow{\text{simulation}} \hat{\rho}_{\text{mag}}. \quad (47)$$

§ A similar correction scheme was followed in [50, 51] by ignoring levels higher than $|2\rangle$ where this effect was not observed.

Finally, we calculate the fidelity of state generation $F[\psi_T] = \langle \psi_T | \hat{\rho}_{\text{mag}}[\psi_T] | \psi_T \rangle$ which can be interpreted as the probability of finding the magnetization in the target state $|\psi_T\rangle$.

We compare the Wigner function of the target state $|\psi_T\rangle$ and the achieved state $\hat{\rho}_{\text{mag}}[\psi_T]$ for some special cases. The Wigner function is defined as

$$W(\beta, \hat{\rho}) = \int \frac{d^2\gamma}{\pi} \text{Tr} \left[\hat{\rho} \exp \left[(\hat{m} - \beta)^\dagger \gamma - \gamma^* (\hat{m} - \beta) \right] \right]. \quad (48)$$

The Wigner function can be interpreted as follows. Define a symmetric product $\{\hat{m}^{\dagger,p} \hat{m}^q\}_S$ as an average over all permutations of p \hat{m}^\dagger 's and q \hat{m} 's. For example,

$$\{\hat{m}^{\dagger,2} \hat{m}\}_S = \frac{\hat{m}^{\dagger,2} \hat{m} + \hat{m}^\dagger \hat{m} \hat{m}^\dagger + \hat{m} \hat{m}^{\dagger,2}}{3}. \quad (49)$$

In a given state $\hat{\rho}$, the average of the above operator is given by [55, 56]

$$\text{Tr} \left[\hat{\rho} \{\hat{m}^{\dagger,p} \hat{m}^q\}_S \right] = \int \frac{d^2\beta}{\pi} \beta^{*,p} \beta^q W(\beta, \hat{\rho}). \quad (50)$$

We can convert this into expectation values of the magnetization operators \hat{M}_x and \hat{M}_y via the substitution $2\mathcal{M}_{\text{ZPF}} \hat{m} \rightarrow \hat{M}_x - i\hat{M}_y$ (note that we are using the dressed operator \hat{m} instead of the bare magnetization operator \hat{M} as the distinction between them is small) getting

$$\text{Tr} \left[\hat{\rho} \{\hat{M}_x^p \hat{M}_y^q\}_S \right] = \int \frac{dM_x dM_y}{\pi} M_x^p M_y^q \tilde{W}(M_x, M_y, \hat{\rho}), \quad (51)$$

where $\tilde{W}(M_x, M_y, \hat{\rho}) = W\left(\frac{M_x - iM_y}{2\mathcal{M}_{\text{ZPF}}}, \hat{\rho}\right)$. The above equation suggests an interpretation of \tilde{W} as a quasi-classical probability distribution. However, note that \tilde{W} is not always positive and a negative \tilde{W} implies a lack of a probabilistic interpretation considered to be a signature of non-classicality. The unit \mathcal{M}_{ZPF} , defined in Eq. (2), is given by

$$\frac{\mathcal{M}_{\text{ZPF}}}{M_s} = 8 \times 10^{-6} \sqrt{\frac{1 \mu\text{m}^3}{V_m}}, \quad (52)$$

where V_m is the volume of the magnet. This is a very small angle but it can be measured via the magnet's coupling to the transmon [31, 32].

In Fig. 4, we consider the case of Fock states $|\psi_{\text{Fock}}(n)\rangle = |n\rangle$ and their superposition with the ground state $|\psi_{\text{Sup}}(n)\rangle \propto |0\rangle + |n\rangle$ where $n \in \{1, 2, \dots, 14\}$. The fidelity decreases with increasing n . This is caused by two factors. The dominant factor is an increase in the protocol time with the number of magnons leading to higher decay. Secondly, each gate introduces a small amount of error, including residual transfer to higher levels, that compounds with the number of gates, linearly increasing with n . It appears that Fock states are more difficult to generate than the superposition states, which could be due to a larger average number of magnons in $|\psi_{\text{Fock}}\rangle$, compared to $|\psi_{\text{Sup}}\rangle$, leading to a faster decay. For $n \in \{6, 10\}$ and $T \in \{\text{Fock}, \text{Sup}\}$, we also show Wigner functions of the target state, $\tilde{W}(M_x, M_y, |\psi_T(n)\rangle \langle \psi_T(n)|)$ and the achieved state $\tilde{W}(M_x, M_y, \hat{\rho}_{\text{mag}}[\psi_T(n)])$. The essential feature of $|\psi_{\text{Sup}}(n)\rangle$ are the azimuthal fringes

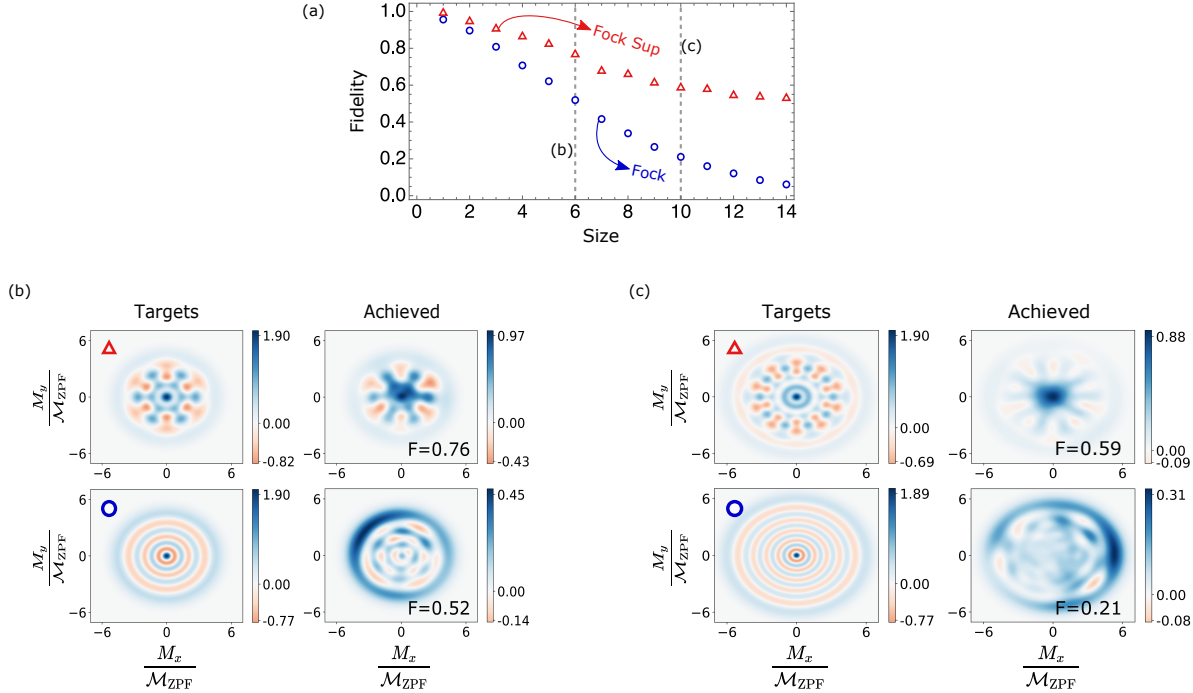


Figure 4. (a) Fidelity of generation for Fock states $|n\rangle$ (blue circles) and superpositions between the vacuum and Fock states $(|0\rangle + |n\rangle)/\sqrt{2}$ (red triangles) as a function of n . Wigner functions of target and achieved state are plotted for $n = 6$ in (b) and $n = 10$ in (c) with fidelity (F) written.

of order n , which is well captured for $n = 6$ and weakly reproduced for $n = 10$. The essential feature of $|\psi_{\text{Fock}}(n)\rangle$ are the n circular fringes, that are destroyed by dephasing.

A superposition of two semi-classical states, known as a cat state, is useful for error correction protocols because of their insensitivity to particle loss noise [57], particularly as carriers of information [58, 59, 60] and in metrology [61, 62, 63, 64]. In case of a magnet, we can define semi-classical states as the minimum-uncertainty states with isotropic quantum fluctuations, given by coherent states [65]

$$|\xi\rangle = e^{-|\xi|^2/2} \sum_{n=0}^{\infty} \frac{\xi^n}{\sqrt{n!}} |n\rangle, \quad (53)$$

for an arbitrary complex number ξ . A coherent state has average $\langle \hat{m} \rangle = \xi$ and can be interpreted as the quantum state ‘closest’ to the classical state with magnetization $M_x = 2\mathcal{M}_{\text{ZPF}}\text{Re}(\xi)$ and $M_y = -2\mathcal{M}_{\text{ZPF}}\text{Im}(\xi)$. An ‘odd’ cat state given by $|\psi_{\text{odd}}(\xi)\rangle \propto |\xi/2\rangle - |-\xi/2\rangle$ has two semi-classical components separated by the magnetization $2\mathcal{M}_{\text{ZPF}}|\xi|$; the same holds for an ‘even’ cat state $|\psi_{\text{even}}(\xi)\rangle \propto |\xi/2\rangle + |-\xi/2\rangle$. Fig. 5 shows the fidelity of generation as a function of ξ . The Wigner function for an ideal cat state has two blobs at the expected peaks along with fringes in the center. The presence of the fringes signify the quantum coherence between the two semi-classical components. In contrast, the Wigner function for a classical distribution, $\hat{\rho}_{\text{cl}}(\xi) \propto |\xi/2\rangle\langle\xi/2| + |-\xi/2\rangle\langle-\xi/2|$ would still have the blobs but no fringes.

In the achieved states, we find such fringes for cat sizes up to 4 until which the

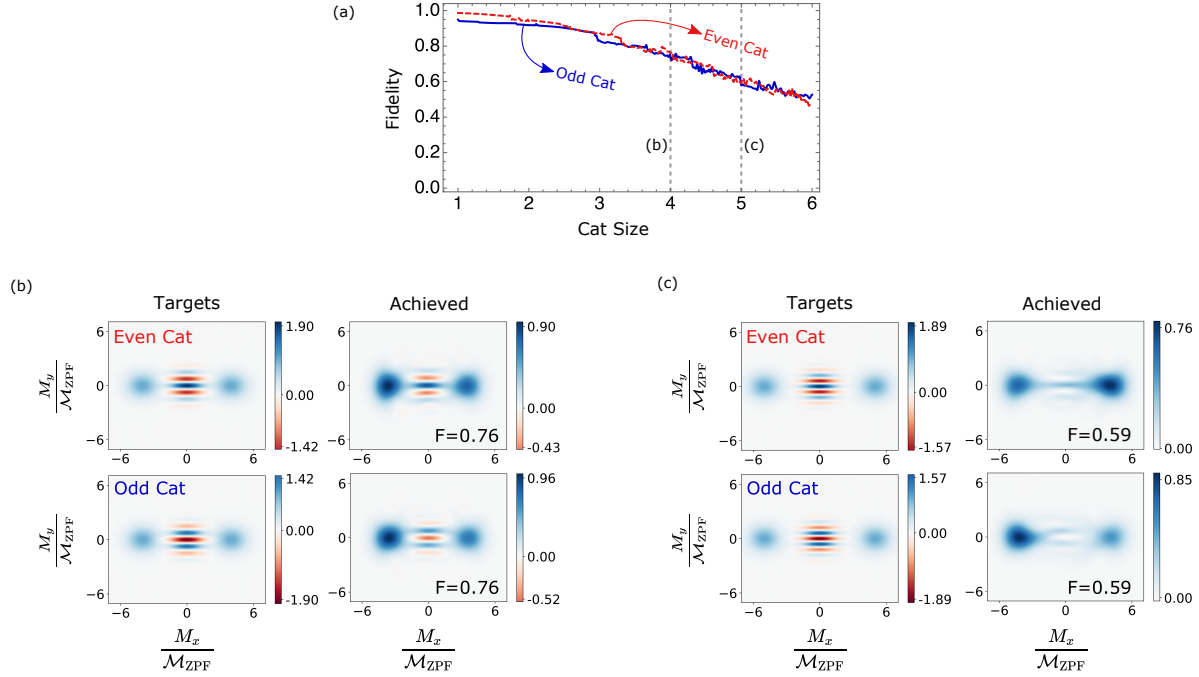


Figure 5. (a) Fidelity of generation for cat states $|\xi/2\rangle \pm |-\xi/2\rangle$ as a function of cat size. Wigner functions of target and achieved state are plotted for $\xi = 4$ in (b) and $\xi = 5$ in (c) with fidelity (F) written.

fidelities are not too low. At cat size 5, we see that the achieved state are closer to a classical probability distribution [they have > 0.85 fidelity with the corresponding classical states $\hat{\rho}_{cl}(\xi = 5)$]. Differences in the odd and cat states for low sizes can be explained on the basis that odd cats have larger number of magnons, $\frac{\xi^2}{4} \frac{1+e^{-\xi^2/2}}{1-e^{-\xi^2/2}}$, than even cats, $\frac{\xi^2}{4} \frac{1-e^{-\xi^2/2}}{1+e^{-\xi^2/2}}$, an effect that is negligible for $\xi > 2$. Fidelity for generation of any other state can be found using the available codes [66].

5. Improvements

Here, we focussed on adapting and characterizing the protocol for a system with a magnet and a transmon. There are several methods by which the protocol can be improved, as we now elaborate.

Pre-processing: We considered only a specific type of operations, where the transmon is excited and the excitation is transferred to the magnons. With the help of the MW cavity, one can also apply other operations, in particular, a displacement given by $\hat{D}(\alpha) = e^{\alpha \hat{m}^\dagger - \alpha^* \hat{m}}$ caused by a coherent excitation of the magnet by MWs. This can be used to decrease the time of the protocol as one can choose an appropriate α , such that $\hat{D}^\dagger(\alpha) |\psi_T\rangle$ has fewer magnons than $|\psi_T\rangle$. For example, if $\langle \psi_T | \hat{m} | \psi_T \rangle = C$, then

$$\langle \psi_T | \hat{D}(C) \hat{m}^\dagger \hat{m} \hat{D}^\dagger(C) | \psi_T \rangle = \langle \psi_T | \hat{m}^\dagger \hat{m} | \psi_T \rangle - |C|^2, \quad (54)$$

implying that $\hat{D}^\dagger(C) |\psi_T\rangle$ has fewer average magnons than $|\psi_T\rangle$. A better α can be found numerically that decreases the highest amplitude in $|\psi_T\rangle$ to within some given

tolerance. Then, we run the protocol to create $\hat{D}^\dagger(\alpha)|\psi_T\rangle$ and apply a MW pulse to displace keeping a high fidelity. If there are other operations that can be easily performed, they can be used for pre-processing to decrease the size.

High fidelity gates: In our analysis, we find that non-ideal transmon gates are responsible for a significant part of fidelity loss which increases linearly with the number of gates necessary to generate the target state. We took a simple case of correcting at first order perturbation similar to [50, 51]. Simply adding higher order terms in a Dyson or a Magnus expansion does not necessarily improve gate fidelities. When we correct for second order term in Magnus expansion, we find that we can decrease the transitions $|0\rangle \leftrightarrow |2\rangle$ and $|1\rangle \leftrightarrow |2\rangle$ significantly, but at the expense of a high $|0\rangle \leftrightarrow |3\rangle$ transition probability \parallel . This gets corrected only at the third order in Magnus expansion, at which point the $|0\rangle \leftrightarrow |4\rangle$ transition might play a role. However, there is a rich literature on speeding up gates to $\sim 2\pi/\alpha$ with low loss of fidelity, such as DRAG [67, 68] or optimal control [69, 70, 71, 72], that can not only speed up but also improve the accuracy of gates.

Combining steps: We followed a semi-analytical approach where we systematically add an excitation one by one. In principle, some steps can be combined, e.g. exciting the transmon and transferring the excitation to magnon can occur simultaneously. This becomes infeasible to handle analytically but relevant pulses can, in principle, be found using optimal control theory. A similar case has been discussed in the two-level approximation [73] for a general harmonic oscillator states with 2 – 3 quanta. Although this approach should result in the least possible errors, it is computationally very expensive and scaling such an approach to high magnon numbers [74, 70] would still require a good initial guess for time-dependent functions describing the transmon driving and the transmon frequency.

6. Conclusions

We proposed and numerically demonstrated a protocol to generate an arbitrary quantum state of the magnetization using its coupling to a superconducting transmon, which is a weakly anharmonic oscillator. The protocol involves repeatedly applying transmon gates and transferring an excitation to the magnons. As longer protocol times lead to higher dissipation, we can improve fidelity of generation by reducing the gate time, t_g , and the transfer time, t_{on} , in the notation of Secs. 2 and 3. Fast gate pulses with duration $\sim 2\pi/\alpha$ (α is defined in Eq. (21)) would imply leakage of excitation into higher transmon levels that can be reduced by modifying the input pulses [47, 69, 70, 67]. We use correction pulses by removing errors at first order in a Magnus expansion, similar to Refs. [50, 51], bringing the gate time down to $3\pi/\alpha$. Correcting for second order term in the expansion does not seem to decrease errors, but rather transfer the population to higher levels. The transfer time, t_{on} , can be reduced with a higher magnon-transmon coupling. As the magnon-MW coupling can reach very high values, it is likely to be

\parallel In Refs. [50, 51], only a three level system was considered which does not have this problem

experimentally feasible to have high magnon-transmon couplings. However, a coupling $g \sim \alpha$ causes leakage of magnons into higher transmon levels leading to loss of fidelities, so we choose $g < 0.1\alpha$. For such couplings, the leakage is small and can be incorporated by renormalizing the duration of the coupling, $t_{\text{on},j}$.

The main source of errors is the magnon dissipation putting a limit on the size of the states. We find that the protocol faithfully produces states up to a largest occupation of ~ 9 magnons and an average of ~ 4 magnons. We note that our protocol creates states in dressed magnons, given by \hat{m} instead of bare magnons \hat{M} . As discussed in Appendix A, for a sufficiently large detuning between MWs and magnons, the distinction is small. We demonstrated our protocol for cases of Fock states $|n\rangle$, Fock superpositions $|0\rangle + |n\rangle$, and cat states $|\alpha\rangle \pm |-\alpha\rangle$. While our protocol gives good fidelities for states of moderate sizes, we expect that advanced numerical techniques such as optimal quantum control [74, 70, 71] can improve the state generation (likely by reducing the protocol time) by using our protocol as an initial guiding guess.

With a setup to generate an arbitrary magnetization, there still lies a question of how to experimentally measure it, which we leave to future work. The figures can be generated via the publicly available codes [66].

Acknowledgements

The authors thank H. Ribeiro for useful discussions. We acknowledge funding from the Max Planck Society and from the Deutsche Forschungsgemeinschaft (DFG, German Research Foundation) through Project-ID 429529648–TRR 306 QuCoLiMa (“Quantum Cooperativity of Light and Matter”).

Appendix A. Derivation of effective Hamiltonian

In this appendix, we derive the effective Hamiltonian for a magnet coupled to a transmon indirectly via a MW cavity.

Appendix A.1. Microwaves

The MW cavity is modeled by the classical Hamiltonian density

$$\mathcal{H}_{\text{mw}} = \frac{\epsilon_0 |\mathbf{E}|^2 + \mu_0 |\mathbf{H}|^2}{2}. \quad (\text{A.1})$$

It contains several modes labelled by r giving the quantization

$$\mathbf{H}(\mathbf{r}) \rightarrow \sum_r \mathbf{H}_r(\mathbf{r}) \hat{A}_r + \mathbf{H}_r^*(\mathbf{r}) \hat{A}_r^\dagger, \quad (\text{A.2})$$

and similar holds for \mathbf{E} . Here, \mathbf{H}_r and \hat{A}_r are respectively the mode profile and the annihilation operator of mode r . With appropriate normalization, this gives the Hamiltonian,

$$\hat{H}_{\text{mw}} = \hbar \sum_r \Omega_{a,r} \hat{A}_r^\dagger \hat{A}_r, \quad (\text{A.3})$$

where $\Omega_{a,r}$ is the resonance frequency of mode r .

Appendix A.2. Magnet

If the magnet is much smaller than MW wavelengths (\sim cm), then only the total magnetization \mathbf{M} couples to the MWs. Under a DC field along \mathbf{z} with magnitude H_{app} , its classical Hamiltonian density is

$$\mathcal{H}_{\text{m,mw}} = -\mu_0 H_{\text{app}} M_z - \mu_0 \mathbf{M} \cdot \mathbf{H}, \quad (\text{A.4})$$

where \mathbf{H} is the magnetic field due to the cavity. The magnetization is quantized by the Holstein-Primakoff transformation [41, 42], given by a form

$$M_x - iM_y \rightarrow 2\mathcal{M}_{\text{ZPF}} \hat{M} \sqrt{\frac{1 - \beta \hat{M}^\dagger \hat{M}}{1 - \beta}}, \quad (\text{A.5})$$

where \mathcal{M}_{ZPF} and β are to be found. We know that a spin in an applied field undergoes a Larmor precession with frequency $\Omega_m = \gamma \mu_0 H_{\text{app}}$ where γ is the absolute value of the gyromagnetic ratio. This implies that the Kittel mode should have the resonance frequency, i.e. after quantization

$$-\mu_0 V_m H_{\text{app}} M_z \rightarrow \hbar \Omega_m \hat{M}^\dagger \hat{M}. \quad (\text{A.6})$$

This implies $M_z = \tilde{M}_s - M_{\text{sing}} \hat{M}^\dagger \hat{M}$ where \tilde{M}_s (to be found) is the saturation magnetization reduced by zero point fluctuations and $M_{\text{sing}} = \gamma \hbar / V_m$ is the magnetization reduction because of one (delocalized) spin flip. Using $M_x^2 + M_y^2 + M_z^2 = M_s^2$, we find the relations

$$\tilde{M}_s^2 + 2\mathcal{M}_{\text{ZPF}}^2 = M_s^2, \quad \mathcal{M}_{\text{ZPF}} = \sqrt{\frac{\tilde{M}_s M_{\text{sing}}}{2}}, \quad M_{\text{sing}}^2 = \frac{4\mathcal{M}_{\text{ZPF}}^2 \beta}{1 - \beta}. \quad (\text{A.7})$$

This is solved explicitly by

$$\tilde{M}_s = \sqrt{M_s^2 + \frac{M_{\text{sing}}^2}{2}} - \frac{M_{\text{sing}}}{2}, \quad \beta = \frac{M_{\text{sing}}}{2\tilde{M}_s + M_{\text{sing}}} \quad (\text{A.8})$$

Typically $M_{\text{sing}}/M_s < 10^{-10}$, so we can resort to the leading order corrections,

$$\tilde{M}_s \approx M_s - \frac{M_{\text{sing}}}{2}, \quad \mathcal{M}_{\text{ZPF}} \approx \sqrt{\frac{M_s M_{\text{sing}}}{2}}, \quad \beta \approx \frac{M_{\text{sing}}}{M_s}. \quad (\text{A.9})$$

For $\langle \hat{M}^\dagger \hat{M} \rangle \ll 1/\beta \sim 10^{10}$, we can simply substitute

$$M_x - iM_y \rightarrow 2\mathcal{M}_{\text{ZPF}} \hat{M}, \quad M_z \rightarrow M_s - \frac{2\mathcal{M}_{\text{ZPF}}^2}{M_s} \hat{M}^\dagger \hat{M}. \quad (\text{A.10})$$

This gives the magnon Hamiltonian (coupled to the cavity)

$$\hat{H}_{\text{m,mw}} = \hbar \Omega_m \hat{M}^\dagger \hat{M} + \sum_r G_{m,r} \hat{M}^\dagger \hat{A}_r + G_{m,r}^* \hat{M} \hat{A}_r^\dagger, \quad (\text{A.11})$$

where $\Omega_m = \gamma \mu_0 H_{\text{app}}$ and

$$\hbar G_{m,r} = -\mu_0 \mathcal{M}_{\text{ZPF}} (H_{x,r} - iH_{y,r}). \quad (\text{A.12})$$

We assumed rotating wave approximation which is valid when $G \ll \Omega_m + \Omega_a$.

Appendix A.3. Transmon

We consider a flux-tunable transmon that consists of two Josephson junctions in parallel forming a SQUID loop. Its Hamiltonian is [45, 44]

$$\hat{H}_{\text{tr,mw}} = E_C (\hat{n} + \hat{n}_{\text{mw}})^2 - E_{J_1} \cos \hat{\phi}_1 - E_{J_2} \cos \hat{\phi}_2. \quad (\text{A.13})$$

Here, \hat{n} is the number of quanta exchanged between the two junctions, \hat{n}_{mw} is the number of quanta excited by MWs, and $\hat{\phi}_{1,2}$ are the fluxes through each junction. Under weak coupling, we have $\hat{n}_{\text{mw}} \propto |\mathbf{E}|$. Flux quantization constraints $\hat{\phi}_1 - \hat{\phi}_2 = 2\pi m + 2\pi\Phi/\Phi_0$ where m is an arbitrary integer, Φ is the flux through the SQUID loop, and $\Phi_0 = h/2e$ is the superconducting flux quantum. Defining $2\hat{\phi} = \hat{\phi}_1 + \hat{\phi}_2$,

$$\hat{H}_{\text{tr}} = E_C \hat{n}^2 - E_{J,\text{eff}} \cos(\hat{\phi} + \phi_0). \quad (\text{A.14})$$

where the phase is

$$\phi_0 = \tan^{-1} \left(\frac{E_{J_1} - E_{J_2}}{E_{J_1} + E_{J_2}} \tan \frac{\pi\Phi}{\Phi_0} \right) + n\pi \quad (\text{A.15})$$

and the effective junction energy is

$$E_{J,\text{eff}}(\Phi) = \sqrt{(E_{J_1} + E_{J_2})^2 \cos^2 \frac{\pi\Phi}{\Phi_0} + (E_{J_1} - E_{J_2})^2 \sin^2 \frac{\pi\Phi}{\Phi_0}}. \quad (\text{A.16})$$

In the transmon limit $E_{J,\text{eff}} \gg E_C$, the fluctuations in $\hat{\phi} + \phi_0$ are small, so we can expand the cosine and get an approximately quadratic Hamiltonian. This suggests the quantization,

$$\hat{n} = \left(\frac{E_{J,\text{eff}}}{2E_C} \right)^{1/4} \frac{\hat{Q} - \hat{Q}^\dagger}{\sqrt{2}i}, \quad \hat{\phi} + \phi_0 = \left(\frac{2E_C}{E_{J,\text{eff}}} \right)^{1/4} \frac{\hat{Q} + \hat{Q}^\dagger}{\sqrt{2}}, \quad (\text{A.17})$$

that reduces the Hamiltonian to

$$\hat{H}_{\text{q,mw}} = \hbar\Omega_q \hat{Q}^\dagger \hat{Q} - \hbar \frac{A}{2} \hat{Q}^\dagger \hat{Q} (\hat{Q}^\dagger \hat{Q} - 1) + \hbar \sum_r (G_{q,r} \hat{Q}^\dagger \hat{A}_r + G_{q,r}^* \hat{Q} \hat{A}_r^\dagger), \quad (\text{A.18})$$

ignoring higher order terms. Here $\hbar\Omega_q = \sqrt{2E_C E_{J,\text{eff}}} - E_C/4$ and $\hbar A = E_C/4$.

Appendix A.4. Dressed magnons and transmons

The dressed states are found by diagonalizing the total Hamiltonian $\hat{H} = \hat{H}_0 + \hat{H}_{\text{int}}$ where

$$\frac{\hat{H}_0}{\hbar} = \sum_r \Omega_{a,r} \hat{A}_r^\dagger \hat{A}_r + \Omega_m \hat{M}^\dagger \hat{M} + \Omega_q \hat{Q}^\dagger \hat{Q} - \frac{A}{2} \hat{Q}^\dagger \hat{Q} (\hat{Q}^\dagger \hat{Q} - 1), \quad (\text{A.19})$$

and the interaction

$$\frac{\hat{H}_{\text{int}}}{\hbar} = \sum_r (G_{m,r} \hat{M}^\dagger \hat{A}_r + G_{m,r}^* \hat{M} \hat{A}_r^\dagger + G_{q,r} \hat{Q}^\dagger \hat{A}_r + G_{q,r}^* \hat{Q} \hat{A}_r^\dagger). \quad (\text{A.20})$$

However, exact diagonalization is not possible analytically, so we resort to a perturbative treatment, in particular a Schrieffer-Wolff (SW) transformation [75]. The SW transformation perturbatively gives the rotation operator $\hat{S} = -\hat{S}^\dagger$ such that $e^{-\hat{S}} \hat{H} e^{\hat{S}}$ is

diagonal to a given order. We find \hat{S} to linear order in coupling constants G that gives the rotated Hamiltonian,

$$e^{-\hat{S}}\hat{H}e^{\hat{S}} = \hat{H}_0 + \hat{H}_{\text{int}} + [\hat{H}_0, \hat{S}] + [\hat{H}_{\text{int}}, \hat{S}] + \frac{1}{2} [[\hat{H}_0, \hat{S}], \hat{S}] + O(G^3). \quad (\text{A.21})$$

To remove first order corrections, we choose

$$\hat{S} = \sum_r \left(\frac{G_{m,r}}{\Omega_{a,r} - \Omega_m} \hat{A}_r \hat{M}^\dagger + G_{q,r} \chi_r [\hat{Q}^\dagger \hat{Q}] \hat{A}_r \hat{Q}^\dagger \right) - h.c. \quad (\text{A.22})$$

where the transmon susceptibility is

$$\chi_r[x] = \frac{1}{\Omega_{a,r} - \Omega_q - \alpha(x-1)}, \quad (\text{A.23})$$

ensuring $\hat{H}_{\text{int}} + [\hat{H}_0, \hat{S}] = \hat{0}$. Note that we need $\|\hat{S}\| \ll 1$ that implies a limit on the number of excitations $\{N_{a,r}, N_m, N_q\}$ s.t. for all r ,

$$G_{m,r} \sqrt{N_{a,r} N_m} \ll \Omega_{a,r} - \Omega_m, \quad G_{q,r} \sqrt{N_{a,r} N_q} \ll \Omega_{a,r} - \Omega_q \quad (\text{A.24})$$

are satisfied. This gives the rotated Hamiltonian,

$$e^{-\hat{S}}\hat{H}e^{\hat{S}} = \hat{H}_0 + \frac{1}{2} [\hat{H}_{\text{int}}, \hat{S}] + O(G^3). \quad (\text{A.25})$$

As there are four terms in both \hat{H}_{int} and \hat{S} , a total of 16 commutators are required. If we ignore all non-resonant terms, such as $\hat{A}_r^2 \hat{Q}^{\dagger,2}$, and use the Hermiticity of \hat{H}_{int} we are left with

$$\frac{1}{2\hbar} [\hat{H}_{\text{int}}, \hat{S}] = \sum_{rs} \left[(G_{m,r}^* \hat{M} + G_{q,r}^* \hat{Q}) \hat{A}_r^\dagger, \left(\frac{G_{m,s}}{\Omega_{a,s} - \Omega_m} \hat{M}^\dagger + G_{q,s} \chi_s (\hat{Q}^\dagger \hat{Q}) \hat{Q}^\dagger \right) \hat{A}_s \right] + h.c. \quad (\text{A.26})$$

For \hat{f}, \hat{g} commuting with all photon operators,

$$[\hat{f} \hat{A}_r^\dagger, \hat{g} \hat{A}_s] = -\hat{f} \hat{g} \delta_{rs} + [\hat{f}, \hat{g}] \hat{A}_r^\dagger \hat{A}_s. \quad (\text{A.27})$$

This leads to

$$\begin{aligned} \frac{1}{2\hbar} [\hat{H}_{\text{int}}, \hat{S}] &= -\sum_r (G_{m,r}^* \hat{M} + G_{q,r}^* \hat{Q}) \left(\frac{G_{m,r}}{\Omega_{a,r} - \Omega_m} \hat{M}^\dagger + G_{q,r} \chi_r (\hat{Q}^\dagger \hat{Q}) \hat{Q}^\dagger \right) \\ &\quad + \delta\Omega_{a,r} [\hat{Q}^\dagger \hat{Q}] \hat{A}_r^\dagger \hat{A}_r + h.c. \end{aligned} \quad (\text{A.28})$$

where

$$\delta\Omega_{a,r}[x] = \frac{|G_{m,r}|^2}{\Omega_{a,r} - \Omega_m} + |G_{q,r}|^2 ((x+1)\chi_r(x+1) - x\chi_r(x)). \quad (\text{A.29})$$

This procedure yields the rotated Hamiltonian. To return back to the original one, we define the dressed operators: $\hat{m} = e^{\hat{S}} \hat{M} e^{-\hat{S}}$, $\hat{q} = e^{\hat{S}} \hat{Q} e^{-\hat{S}}$, and $\hat{a}_r = e^{\hat{S}} \hat{A}_r e^{-\hat{S}}$. Up to linear order in G , the dressed magnon operator is

$$\hat{m} \approx \hat{M} - \sum \frac{G_{m,r}}{\Omega_{a,r} - \Omega_m} \hat{A}_r + O(G^2), \quad (\text{A.30})$$

and the dressed transmon operator is

$$\hat{q} \approx \hat{Q} - \sum G_{q,r} \hat{A}_r (\chi_r [\hat{Q} \hat{Q}^\dagger] - \chi_r [\hat{Q}^\dagger \hat{Q}]) + O(G^2). \quad (\text{A.31})$$

This gives the final Hamiltonian

$$\frac{\hat{H}}{\hbar} = \omega_m \hat{m}^\dagger \hat{m} + (\omega_q + \hat{\alpha} [\hat{q}^\dagger \hat{q}]) \hat{q}^\dagger \hat{q} + \hat{m} \hat{q}^\dagger \hat{g} [\hat{q}^\dagger \hat{q}] + \hat{g} [\hat{q}^\dagger \hat{q}] \hat{m}^\dagger \hat{q} + \frac{\hat{H}_{\text{mw,eff}}}{\hbar}. \quad (\text{A.32})$$

Here, $\hat{H}_{\text{mw,eff}}$ is the effective MW Hamiltonian that is not relevant for our discussion. The renormalized magnon's frequency is Stark shifted by the MWs:

$$\omega_m = \Omega_m - \sum_r \frac{|G_{m,r}|^2}{\Omega_{a,r} - \Omega_m}. \quad (\text{A.33})$$

Similarly, the transmon's frequency is

$$\omega_q = \Omega_q - \sum_r \frac{|G_{q,r}|^2}{\Omega_{a,r} - \Omega_q}. \quad (\text{A.34})$$

The Stark shift of higher transmon levels renormalizes the anharmonicity to

$$\hat{\alpha} [\hat{q}^\dagger \hat{q}] = \frac{A}{2} (\hat{q}^\dagger \hat{q} - 1) - \sum_r |G_{q,r}|^2 \left[\frac{1}{\Omega_{a,r} - \Omega_q - A (\hat{q}^\dagger \hat{q} - 1)} - \frac{1}{\Omega_{a,r} - \Omega_q} \right]. \quad (\text{A.35})$$

Finally, the coupling of each transmon transition to the magnons is given by

$$\hat{g} [\hat{q}^\dagger \hat{q}] = -\frac{1}{2} \sum_r G_{m,r}^* G_{q,r} \left(\frac{1}{\Omega_{a,r} - \Omega_q - A \hat{q}^\dagger \hat{q}} + \frac{1}{\Omega_{a,r} - \Omega_m} \right). \quad (\text{A.36})$$

Appendix B. Transfer of Quanta

In this appendix, we show how to obtain the periods required for transferring quanta from transmon to magnons. In what follows, $|m, q\rangle$ denotes a state with m magnons and transmon at q th level. Given a state $|\Psi\rangle$ having a maximum of j excitations, i.e. $\langle m, q | \Psi \rangle = 0$ for $m + q > j$ and a tunable Hamiltonian

$$\frac{\hat{H}(t)}{\hbar} = \omega_m \hat{m}^\dagger \hat{m} + (\omega_q + \Delta(t)) \hat{q}^\dagger \hat{q} - \sum_{n=2}^{\infty} \alpha_n |n\rangle \langle n| + \sum_{n=0}^{\infty} g_n \hat{m}^\dagger |n\rangle \langle n+1| + g_n^* \hat{m} |n+1\rangle \langle n|, \quad (\text{B.1})$$

we want to find $\{\Delta(t), t_{\text{tot}}\}$ s.t. $\langle j, 0 | \hat{\mathcal{T}}^\dagger | \Psi \rangle = 0$, where the time-evolution operator is

$$\hat{\mathcal{T}} = \text{Texp} \left[-\frac{i}{\hbar} \int_0^{t_{\text{tot}}} \hat{H}(\tau) d\tau \right], \quad (\text{B.2})$$

with Texp being the time-ordered exponential operator. Here, $\alpha_n \equiv \langle n | \hat{\alpha} | n \rangle$ and $g_n \equiv \langle n | \hat{g} | n \rangle$ as derived in the previous section.

First, consider the ansatz $\Delta(t) = \Delta_0 [u(t - t_{\text{on}}) - u(t)]$ with $\Delta_0 = \omega_m - \omega_q$, s.t. the magnons and transmons are resonant for a time-period t_{on} , effectively switching on the coupling. Adding an off-period of t_{off} afterwards, we get $t_{\text{tot}} = t_{\text{on}} + t_{\text{off}}$ and we want to find $\{t_{\text{on}}, t_{\text{off}}\}$ to satisfy the above condition. We can derive the time-evolution unitary explicitly using $[\hat{H}(t), \hat{N}] = 0$ where the total number of excitations are given by

$$\hat{N} = \hat{m}^\dagger \hat{m} + \hat{q}^\dagger \hat{q}. \quad (\text{B.3})$$

Thus, we divide the wave-function as

$$|\Psi(t)\rangle = \sum_{N=0}^{\infty} \sum_{s=0}^N \xi_{Ns}(t) |N - s, s\rangle. \quad (\text{B.4})$$

During the off-time, we have the equations of motion, [using the Schrödinger equation $|\dot{\Psi}\rangle = -i\hat{H}|\Psi\rangle$].

$$\dot{\xi}_{Ns} = -i(\omega_m(N-s) + \omega_qs - \alpha_s)\xi_{Ns} - i[g_s\sqrt{N-s}\xi_{N,s+1} + g_{s-1}^*\sqrt{N-s+1}\xi_{N,s-1}]. \quad (\text{B.5})$$

This is a set of linear differential equations which can be solved by diagonalizing the dynamical matrix. For the case $N = j$, we can write

$$\xi_j(t_{\text{on}} + t_{\text{off}}) = V_{\text{off}}e^{-i\Lambda_{\text{off}}t_{\text{off}}}V_{\text{off}}^\dagger\xi_j(t_{\text{on}}), \quad (\text{B.6})$$

where the vector $\xi_j = (\xi_{j0} \ \xi_{j1} \ \dots \ \xi_{jj})^T$, and the dynamical matrix is diagonalized by $\{-i\Lambda_{\text{off}}, V_{\text{off}}\}$. Similar analysis with $\omega_q \rightarrow \omega_m$ works for the on-time,

$$\xi_j(t_{\text{on}} + t_{\text{off}}) = V_{\text{off}}e^{-i\Lambda_{\text{off}}t_{\text{off}}}V_{\text{off}}^\dagger V_{\text{on}}e^{-i\Lambda_{\text{on}}t_{\text{on}}}V_{\text{on}}^\dagger\xi_j(0). \quad (\text{B.7})$$

We want to ensure $\langle\Psi|\hat{\mathcal{T}}|j, 0\rangle = 0$. We find $\hat{\mathcal{T}}|j, 0\rangle$ by putting $\xi_j(0) = (1 \ 0 \ \dots \ 0)^T \equiv \mathbf{u}_j$ and then, the condition $\langle\Psi|\hat{\mathcal{T}}|j, 0\rangle = 0$ becomes

$$\Psi_j^\dagger \left(V_{\text{off}}e^{-i\Lambda_{\text{off}}t_{\text{off}}}V_{\text{off}}^\dagger V_{\text{on}}e^{-i\Lambda_{\text{on}}t_{\text{on}}}V_{\text{on}}^\dagger \right) \mathbf{u}_j = 0, \quad (\text{B.8})$$

where the vector $\Psi_j = (\langle j, 0|\Psi\rangle \ \langle j-1, 1|\Psi\rangle \ \dots \ \langle 0, j|\Psi\rangle)^T$. This can be numerically solved for $\{t_{\text{on}}, t_{\text{off}}\}$.

In the special case of a two-level approximation (ignoring higher levels) and for sufficiently large detuning $g_0 \ll \omega_m - \omega_q$, the above condition reduces to

$$\cos\left(g_0t_{\text{on}}^{(0)}\sqrt{j}\right)\langle j, 0|\Psi\rangle + ie^{-i\Delta_0t_{\text{off}}^{(0)}}\sin\left(g_0t_{\text{on}}^{(0)}\sqrt{j}\right)\langle j-1, 1|\Psi\rangle = 0. \quad (\text{B.9})$$

This gives

$$g_0\sqrt{j}t_{\text{on}}^{(0)} = \tan^{-1}\left|\frac{\langle j, 0|\Psi\rangle}{\langle j-1, 1|\Psi\rangle}\right|, \quad (\text{B.10})$$

$$\Delta_0t_{\text{off}}^{(0)} = \arg\left[\frac{\langle j, 0|\Psi\rangle}{\langle j-1, 1|\Psi\rangle}\right] + \frac{\pi}{2}. \quad (\text{B.11})$$

In some special cases, Eq. (B.8) will have no solution. Then, we try the ansatz with a pulse of width $t_{\text{on}}^{(0)}$, followed by an off-time $t_{\text{off}}^{(0)}$ and a second pulse of an undetermined time t_{on} ,

$$\Delta(t) = \Delta_0\left[u\left(t - t_{\text{on}} - t_{\text{tot}}^{(0)}\right) - u\left(t - t_{\text{tot}}^{(0)}\right) + u\left(t - t_{\text{on}}^{(0)}\right) - u(t)\right], \quad (\text{B.12})$$

where $t_{\text{tot}}^{(0)} = t_{\text{on}}^{(0)} + t_{\text{off}}^{(0)}$. After another off-period of time t_{off} , the optimization condition becomes (following the same analysis as before)

$$\Psi_j^\dagger \left(V_{\text{off}}e^{-i\Lambda_{\text{off}}t_{\text{off}}}V_{\text{off}}^\dagger V_{\text{on}}e^{-i\Lambda_{\text{on}}t_{\text{on}}}V_{\text{on}}^\dagger \right) \left(V_{\text{off}}e^{-i\Lambda_{\text{off}}t_{\text{off}}^{(0)}}V_{\text{off}}^\dagger V_{\text{on}}e^{-i\Lambda_{\text{on}}t_{\text{on}}^{(0)}}V_{\text{on}}^\dagger \right) \mathbf{u}_j = 0, \quad (\text{B.13})$$

which can be solved for $\{t_{\text{on}}, t_{\text{off}}\}$. This process can be repeated indefinitely, however, in practice, we did not observe the need to go beyond a second iteration.

Appendix C. Transmon Gates

We now describe how the transmon gates can be implemented in our scheme. In what follows, $|m, q\rangle$ denotes a state with m magnons and transmon at q th level. Given an initial state $|\Psi\rangle$ with a maximum of j magnons and $(j+1)$ excitations, i.e. $\langle m, q|\Psi\rangle = 0$ for $m+q > j+1$ and $\langle j+1, 0|\Psi\rangle = 0$, and a tunable Hamiltonian

$$\frac{\hat{H}(t)}{\hbar} = \omega_m \hat{m}^\dagger \hat{m} + \omega_q \hat{q}^\dagger \hat{q} - \sum_{n=2}^{\infty} \alpha_n |n\rangle \langle n| + \tilde{\varepsilon}(t) \hat{q}^\dagger + \tilde{\varepsilon}^*(t) \hat{q}, \quad (\text{C.1})$$

we want to find $\tilde{\varepsilon}(t)$ s.t. $\langle j, 1|\hat{Q}^\dagger|\Psi\rangle = 0$, where the time-evolution operator

$$\hat{Q} = \text{Texp} \left[-\frac{i}{\hbar} \int_0^{t_g} \hat{H}(\tau) d\tau \right], \quad (\text{C.2})$$

with Texp being the time ordered exponential operator and t_g being a pre-determined gate time.

Note that we have ignored the coupling between magnons and transmons assuming large enough detuning $\omega_m - \omega_q$. Then, the evolution is given by

$$\hat{Q}(t) = e^{-i\omega_m t \hat{m}^\dagger \hat{m}} \otimes \hat{U}_g(t). \quad (\text{C.3})$$

Here,

$$\frac{d}{dt} \hat{U}_g = -i \left(\omega_q \hat{q}^\dagger \hat{q} - \sum_{n=2}^{\infty} \alpha_n |n\rangle \langle n| + \tilde{\varepsilon}(t) \hat{q}^\dagger + \tilde{\varepsilon}^*(t) \hat{q} \right) \hat{U}_g. \quad (\text{C.4})$$

An ideal gate between $|0\rangle$ and $|1\rangle$, with angular parameters $\{\theta, \phi\}$ is

$$\hat{U}_{\text{ideal}} = e^{i\Phi_{\text{global}}} \left[\cos \theta (|0\rangle \langle 0| + |1\rangle \langle 1|) + i \sin \theta (e^{i\phi} |1\rangle \langle 0| + e^{-i\phi} |0\rangle \langle 1|) + \sum_{n=2}^{\infty} |n\rangle \langle n| \right], \quad (\text{C.5})$$

barring an unimportant global phase Φ_{global} . The parameters for this gate can be found by ensuring $\langle j, 1|\hat{Q}_{\text{ideal}}^\dagger|\Psi\rangle = 0$, where $\hat{Q}_{\text{ideal}} = e^{-i\omega_m t_g \hat{m}^\dagger \hat{m}} \otimes \hat{U}_{\text{ideal}}$ giving

$$\theta_{\text{ideal}} = \tan^{-1} \left| \frac{\langle j, 1|\Psi\rangle}{\langle j, 0|\Psi\rangle} \right| \quad (\text{C.6})$$

and

$$\phi_{\text{ideal}} = -\frac{\pi}{2} + \arg \left[\frac{\langle j, 1|\Psi\rangle}{\langle j, 0|\Psi\rangle} \right]. \quad (\text{C.7})$$

To implement this, we try the ansatz $\tilde{\varepsilon}(t) = -\varepsilon(t) e^{-i\omega_q t + i\phi_{\text{app}}}$ with real $\{\varepsilon(t), \phi_{\text{app}}\}$ to be found. We separate out the phases by the transformation,

$$\hat{U}_g(t) = e^{-i(\omega_q \hat{q}^\dagger \hat{q} - \sum_{n=2}^{\infty} \alpha_n |n\rangle \langle n|) t} \hat{U}_{\text{ph}} \hat{U}_\theta(t) \hat{U}_{\text{ph}}^\dagger, \quad (\text{C.8})$$

where

$$\hat{U}_{\text{ph}} = e^{i\phi_{\text{app}} \hat{q}^\dagger \hat{q}} \quad (\text{C.9})$$

and \hat{U}_θ satisfies

$$\frac{d}{dt} \hat{U}_\theta = i\varepsilon(t) \left(\sum_{n=0}^{\infty} \sqrt{n+1} e^{-i(\alpha_{n+1} - \alpha_n)t} |n+1\rangle \langle n| + h.c. \right) \hat{U}_\theta, \quad (\text{C.10})$$

where by definition $\alpha_0 = \alpha_1 = 0$.

First, consider the two-level approximation, where we want to solve

$$\frac{d}{dt}\hat{\mathcal{U}}_\theta^{(0)} = i\varepsilon^{(0)}(t) (|0\rangle\langle 1| + |1\rangle\langle 0|)\hat{\mathcal{U}}_\theta^{(0)}, \quad (\text{C.11})$$

where $\varepsilon^{(0)}(t)$ is the ‘bare’ solution to be chosen. The unitary becomes

$$\hat{\mathcal{U}}_\theta^{(0)}(t) = \cos\Theta(t) (|0\rangle\langle 0| + |1\rangle\langle 1|) + i\sin\Theta(t) (|1\rangle\langle 0| + |0\rangle\langle 1|) + \sum_{n=2}^{\infty} |n\rangle\langle n|, \quad (\text{C.12})$$

where

$$\Theta^{(0)}(t) = \int_0^t \varepsilon^{(0)}(\tau) d\tau. \quad (\text{C.13})$$

For such a case, we have

$$\begin{aligned} \hat{\mathcal{U}}_g^{(0)}(t) = & \left[\cos\Theta^{(0)}(t) (|0\rangle\langle 0| + e^{-i\omega_q t_g} |1\rangle\langle 1|) + \right. \\ & \left. i\sin\Theta^{(0)}(t) \left(e^{i\phi_{\text{app}}^{(0)}} e^{-i\omega_q t_g} |1\rangle\langle 0| + e^{-i\phi_{\text{app}}^{(0)}} |0\rangle\langle 1| \right) + \sum_{n=2}^{\infty} e^{-i(\omega_q - \alpha_n)t} |n\rangle\langle n| \right]. \end{aligned}$$

This resembles the ideal gate $\hat{\mathcal{U}}_{\text{ideal}}$ except for the extra phases due to the free evolution of the states. For this two-level approximation, we can ensure $\langle j, 1 | \hat{\mathcal{Q}}^{(0)\dagger} | \tilde{\Psi}_{j+1} \rangle = 0$, where $\hat{\mathcal{Q}}^{(0)} = e^{-i\omega_m t_g \hat{m}^\dagger \hat{m}} \otimes \hat{\mathcal{U}}_g^{(0)}(t_g)$ by choosing

$$\Theta^{(0)}(t_g) = \theta_{\text{ideal}}, \quad \phi_{\text{app}}^{(0)} = \phi_{\text{ideal}} + \omega_q t_g. \quad (\text{C.14})$$

Notice that we can choose any $\varepsilon^{(0)}(t)$ satisfying $\int_0^{t_g} d\tau \varepsilon^{(0)}(\tau) = \theta_{\text{ideal}}$. For concreteness, we choose a sinusoidal

$$\varepsilon^{(0)}(t) = \frac{\pi\theta_{\text{ideal}}}{2t_g} \sin\left(\frac{\pi t}{t_g}\right). \quad (\text{C.15})$$

Appendix C.1. Including all levels

Transition between $|1\rangle$ and $|2\rangle$ are non-resonant by the frequency α_2 , so the above two-level approximation works when $t_g \gg \alpha_2$ [assuming that the anharmonicity increases with levels, i.e. $\alpha_2 < \alpha_3 < \alpha_4 < \dots$]. For a general t_g , we modify the pulse $\varepsilon(t) = \varepsilon^{(0)}(t) + \varepsilon^{(1)}(t)$ and define the error as $\hat{\mathcal{U}}_\theta = \hat{\mathcal{U}}_\theta^{(0)} \hat{\mathcal{U}}_{\text{err}}$. The error satisfies

$$\frac{d\hat{\mathcal{U}}_{\text{err}}}{dt} = i\delta\hat{H} \hat{\mathcal{U}}_{\text{err}}, \quad (\text{C.16})$$

where the error Hamiltonian is

$$\delta\hat{H} = \hat{\mathcal{U}}_\theta^{(0)\dagger} \left(\varepsilon(t) \sum_{n=0}^{\infty} \sqrt{n+1} e^{-i(\alpha_{n+1} - \alpha_n)t} |n+1\rangle\langle n| - \varepsilon^{(0)}(t) (|0\rangle\langle 1| + |1\rangle\langle 0|) + h.c. \right) \hat{\mathcal{U}}_\theta^{(0)}. \quad (\text{C.17})$$

This can be divided as

$$\delta\hat{H} = \left[\varepsilon(t) (\delta\hat{h}_{12} + \delta\hat{h}_{\text{rest}}) + (\varepsilon(t) - \varepsilon^{(0)}(t)) \delta\hat{h}_{01} \right] \quad (\text{C.18})$$

with the reduced Hamiltonians defined as

$$\begin{aligned}\delta\hat{h}_{01} &= |0\rangle\langle 1| + |1\rangle\langle 0| \\ \delta\hat{h}_{12} &= \sqrt{2} e^{-i\alpha_2 t} [\cos\Theta(t) |2\rangle\langle 1| + i \sin\Theta(t) |2\rangle\langle 0|] + h.c. \\ \delta\hat{h}_{\text{rest}} &= \sum_{n=2}^{\infty} \sqrt{n+1} e^{-i(\alpha_{n+1}-\alpha_n)t} |n+1\rangle\langle n| + h.c.\end{aligned}$$

We perform a Magnus expansion to find [50, 51]

$$\hat{\mathcal{U}}_{\text{err}}(t) = \exp \left[i \int_0^t d\tau \delta\hat{H}(\tau) - \frac{1}{2} \int_0^t d\tau_1 \int_0^{\tau_1} d\tau_2 [\delta\hat{H}(\tau_1), \delta\hat{H}(\tau_2)] + \dots \right], \quad (\text{C.19})$$

so, to ensure $\hat{\mathcal{U}}_{\text{err}}(t_g) \approx \hat{I}$ up to first order, we require $\int_0^{t_g} d\tau \delta\hat{H}(\tau) = \hat{0}$ which translates to

$$\int_0^{t_g} \varepsilon(\tau) d\tau = \theta_{\text{ideal}}, \quad (\text{C.20})$$

$$\int_0^{t_g} \varepsilon(\tau) e^{iA_2\tau \pm i\Theta(t)} d\tau = 0, \quad (\text{C.21})$$

$$\int_0^{t_g} \varepsilon(\tau) e^{i(A_3-A_2)\tau} d\tau = 0. \quad (\text{C.22})$$

We used $\int_0^{t_g} \varepsilon^{(0)} d\tau = \theta_{\text{ideal}}$. The last condition ensures that there are no $|2\rangle \leftrightarrow |3\rangle$ transitions, and we ignored all higher transitions as they are approximately unoccupied throughout the protocol.

Appendix C.2. Satisfying the conditions

The conditions allow for a lot of freedom in choosing $\varepsilon(t)$. Here, we take an ansatz of a sum of sinusoids, ensuring that the pulse starts and ends at 0,

$$\varepsilon(t) = \sum_{\nu} \varepsilon_{\nu} \sin\left(\frac{\nu\pi t}{t_g}\right), \quad (\text{C.23})$$

where the set of indices ν can be freely chosen. Eq. (C.20) reads

$$\sum_{\nu \text{ odd}} \frac{2\varepsilon_{\nu} t_g}{\pi\nu} = \theta_{\text{ideal}}. \quad (\text{C.24})$$

Eq. (C.22) is

$$\sum_{\nu} \frac{\pi\nu\varepsilon_{\nu} t_g}{(\alpha_3 - \alpha_2)^2 t_g^2 - \pi^2\nu^2} \left(1 - (-1)^{\nu} e^{i(\alpha_3 - \alpha_2)t_g}\right) = 0. \quad (\text{C.25})$$

Eq. (C.21) is

$$e^{\pm i\theta/2} \sum_{\nu} \frac{\varepsilon_{\nu} t_g}{\pi} \int_0^{\pi} du \sin(\nu u) \exp\left[i\frac{\alpha_2 t_g}{\pi} u \mp \frac{i\theta}{2} \cos u\right] = 0. \quad (\text{C.26})$$

To simplify the integration, we define a real integral

$$G_{\zeta}(\xi) = \int_0^{\pi/2} du \cos[\zeta u - \xi \sin u] \quad (\text{C.27})$$

giving

$$\int_0^{\pi} du \exp[i\zeta u + i\xi \cos u] = 2i^{\zeta} G_{\zeta}(\xi). \quad (\text{C.28})$$

For $\zeta = A_2 t_g / \pi$, this gives

$$0 = \sum_{\nu \text{ odd}} i^{\nu-1} \frac{\varepsilon_\nu t_g}{\pi} \left[G_{\zeta+\nu} \left(\frac{\pm\theta}{2} \right) + G_{\zeta-\nu} \left(\frac{\pm\theta}{2} \right) \right] \quad (\text{C.29})$$

$$= \sum_{\nu \text{ even}} i^\nu \frac{\varepsilon_\nu t_g}{\pi} \left[G_{\zeta+\nu} \left(\frac{\pm\theta}{2} \right) - G_{\zeta-\nu} \left(\frac{\pm\theta}{2} \right) \right]. \quad (\text{C.30})$$

If we choose the gate time s.t. $(A_3 - A_2) t_g = 2N\pi$ for some integer N , we find that the odd and even frequency components can be separated, and in particular, we need only the odd components to satisfy all the above conditions.

For simulation purposes, we choose the specific case of $A_n = An(n-1)/2$, the bare transmon, and choose $At_g = N\pi$ for some natural number N giving (for some arbitrary set of indices H),

$$\varepsilon(t) = \sum_{\mu \in H} \varepsilon_\mu \sin \left(\frac{(2\mu+1)\pi t}{t_g} \right) \quad (\text{C.31})$$

$$\frac{\pi\theta_{\text{ideal}}}{2t_g} = \sum_{\mu \in H} \frac{\varepsilon_\mu}{2\mu+1} \quad (\text{C.32})$$

$$0 = \sum_{\mu \in H} \frac{(2\mu+1)\varepsilon_\mu}{4N^2 - (2\mu+1)^2} \quad (\text{C.33})$$

$$0 = \sum_{\mu \in H} (-1)^\mu \varepsilon_\mu \frac{G_{N+2\mu+1}(\pm\theta/2) + G_{N-2\mu-1}(\pm\theta/2)}{2} \quad (\text{C.34})$$

This is a set of linear equations which can be solved to give ε_μ . To find an expression for $G_n(\theta)$, we use the fact that it satisfies the same recursion relation as that of Bessel functions

$$2G'_n(\xi) = G_{n-1}(\xi) - G_{n+1}(\xi) \quad (\text{C.35})$$

with the initial conditions,

$$G_0(\xi) - \frac{\pi}{2} J_0(\xi) = 0, \quad G_1(\xi) - \frac{\pi}{2} J_1(\xi) = \frac{\sin \xi}{\xi}. \quad (\text{C.36})$$

Then, an expression for $G_n(\xi) - \pi J_n(\xi)/2$ can be found recursively.

Appendix C.3. Phase

Given $\varepsilon(t)$, we find ϕ_{app} to minimize $|\langle j, 1 | \hat{\mathcal{Q}}^\dagger | \Psi \rangle|$. We have $\hat{\mathcal{Q}}(t) = e^{-i\omega_m t \hat{m}^\dagger \hat{m}} \otimes \hat{\mathcal{U}}_g(t)$ where $\hat{\mathcal{U}}_g(t)$ can be decomposed as in Eq. (C.8)]. Then,

$$\hat{\mathcal{U}}_g(t_g) |1\rangle = e^{-i\phi_{\text{app}}} e^{-i(\omega_q \hat{q}^\dagger \hat{q} - \sum_{n=2}^{\infty} \alpha_n |n\rangle \langle n|) t_g} \hat{\mathcal{U}}_{\text{ph}} \hat{\mathcal{U}}_\theta(t_g) |1\rangle. \quad (\text{C.37})$$

As the leakage into higher levels is suppressed via an appropriate choice of $\varepsilon(t)$, we expect the 2x2 sub-block of $\hat{\mathcal{U}}_g(t_g)$ for the subspace spanned by $\{|0\rangle, |1\rangle\}$ to be approximately unitary. For concreteness, we find the unitary matrix closest to this sub-block, say $\hat{\mathcal{U}}_{g,01}$, in 2-norm via $\hat{\mathcal{U}}_{g,01}^{\text{unit}} = VW^\dagger$ using the singular value decomposition $\hat{\mathcal{U}}_{g,01} = V\Lambda W^\dagger$. This gives

$$\hat{\mathcal{U}}_{g,01}^{\text{unit}} |1\rangle = e^{i\Phi_G} \left(i \sin \tilde{\theta} e^{i\delta\phi} |0\rangle + \cos \tilde{\theta} |1\rangle \right), \quad (\text{C.38})$$

for some constants $\{\Phi_G, \tilde{\theta}, \delta\phi\}$. Then,

$$\langle \Psi | \hat{U}_g(t_g) | j, 1 \rangle \approx e^{-ij\omega_m t - i\phi_{\text{app}} + i\Phi_G} \left(i \sin \tilde{\theta} e^{i\delta\phi} \langle \Psi | j, 0 \rangle + \cos \tilde{\theta} e^{i\phi_{\text{app}} - i\omega_q t_g} \langle \Psi | j, 1 \rangle \right), \quad (\text{C.39})$$

giving the amplitude

$$\left| \langle \Psi | \hat{U}_g(t_g) | j, 1 \rangle \right| \approx \sqrt{|\langle \Psi | j, 0 \rangle|^2 + |\langle \Psi | j, 1 \rangle|^2} \left| \cos \theta_{\text{ideal}} \sin \tilde{\theta} - \cos \tilde{\theta} \sin \theta_{\text{ideal}} e^{i\phi_{\text{app}} - i\phi_{\text{app}}^{(0)} - i\delta\phi} \right|. \quad (\text{C.40})$$

This is minimized at

$$\phi_{\text{app}} = \phi_{\text{app}}^{(0)} + \delta\phi. \quad (\text{C.41})$$

Appendix C.4. Gates between higher levels

Typically, there would be leakage from magnons into higher levels of transmon, which needs to be corrected via applying gates between the higher levels. Consider the case when we want to apply a gate between $|n\rangle$ and $|n+1\rangle$ with angular parameters $\{\theta, \phi\}$. We try for a pulse shape

$$\tilde{\varepsilon}(t) = -\frac{\varepsilon(t)}{\sqrt{n}} e^{i\phi_{\text{app}}} e^{-i(n\omega_m - \alpha_n)t}. \quad (\text{C.42})$$

Again, we have the ‘bare’ pulse $\varepsilon^{(0)}$ which we take as half-sines. To remove the errors at first order in the Magnus expansion, we find that $\varepsilon(t)$ here satisfies the same set of conditions Eqs. (C.20)-(C.22). Thus, the same calculations as above apply.

References

- [1] L. J. Cornelissen, J. Liu, R. A. Duine, J. Ben Youssef, and B. J. van Wees. Long-distance transport of magnon spin information in a magnetic insulator at room temperature. *Nat Phys*, 11(12):1022–1026, Dec 2015.
- [2] Y. Kajiwara, K. Harii, S. Takahashi, J. Ohe, K. Uchida, M. Mizuguchi, H. Umezawa, H. Kawai, K. Ando, K. Takanashi, S. Maekawa, and E. Saitoh. Transmission of electrical signals by spin-wave interconversion in a magnetic insulator. *Nature*, 464(7286):262–266, Mar 2010.
- [3] A. V. Chumak, V. I. Vasyuchka, A. A. Serga, and B. Hillebrands. Magnon spintronics. *Nat Phys*, 11(6):453–461, Jun 2015.
- [4] Yutaka Tabuchi, Seiichiro Ishino, Atsushi Noguchi, Toyofumi Ishikawa, Rekishu Yamazaki, Koji Usami, and Yasunobu Nakamura. Quantum magnonics: The magnon meets the superconducting qubit. *Comptes Rendus Physique*, 17(7):729 – 739, 2016. Quantum microwaves / Micro-ondes quantiques.
- [5] H. Y. Yuan, Yunshan Cao, Akashdeep Kamra, Rembert A. Duine, and Peng Yan. Quantum magnonics: when magnon spintronics meets quantum information science. *arXiv:2111.14241 [cond-mat, physics:physics, physics:quant-ph]*, November 2021. arXiv: 2111.14241.
- [6] Yu. M. Bunkov. Quantum Magnonics. *Journal of Experimental and Theoretical Physics*, 131(1):18–28, July 2020.
- [7] A. V. Chumak, P. Kabos, M. Wu, C. Abert, C. Adelman, A. Adeyeye, J. Åkerman, F. G. Aliev, A. Anane, A. Awad, C. H. Back, A. Barman, G. E. W. Bauer, M. Becherer, E. N. Beginin, V. A. S. V. Bittencourt, Y. M. Blanter, P. Bortolotti, I. Boventer, D. A. Bozhko, S. A. Bunyaev, J. J. Carmiggelt, R. R. Cheenikundil, F. Ciubotaru, S. Cotofana, G. Csaba, O. V. Dobrovolskiy, C. Dubs, M. Elyasi, K. G. Fripp, H. Fulara, I. A. Golovchanskiy, C. Gonzalez-Ballester, P. Graczyk, D. Grundler, P. Gruszecki, G. Gubbiotti, K. Guslienko, A. Haldar, S. Hamdioui, R. Hertel, B. Hillebrands, T. Hioki, A. Houshang, C. M. Hu, H. Huebl, M. Huth,

- E. Iacocca, M. B. Jungfleisch, G. N. Kakazei, A. Khitun, R. Khymyn, T. Kikkawa, M. Kläui, O. Klein, J. W. Klos, S. Knauer, S. Koraltan, M. Kostylev, M. Krawczyk, I. N. Krivorotov, V. V. Kruglyak, D. Lachance-Quirion, S. Ladak, R. Lebrun, Y. Li, M. Lindner, R. Macêdo, S. Mayr, G. A. Melkov, S. Mieszczak, Y. Nakamura, H. T. Nembach, A. A. Nikitin, S. A. Nikitov, V. Novosad, J. A. Otalora, Y. Otani, A. Papp, B. Pigeau, P. Pirro, W. Porod, F. Porrati, H. Qin, B. Rana, T. Reimann, F. Riente, O. Romero-Isart, A. Ross, A. V. Sadovnikov, A. R. Safin, E. Saitoh, G. Schmidt, H. Schultheiss, K. Schultheiss, A. A. Serga, S. Sharma, J. M. Shaw, D. Suess, O. Surzhenko, K. Szulc, T. Taniguchi, M. Urbánek, K. Usami, A. B. Ustinov, T. van der Sar, S. van Dijken, V. I. Vasyuchka, R. Verba, S. Viola Kusminskiy, Q. Wang, M. Weides, M. Weiler, S. Wintz, S. P. Wolski, and X. Zhang. Roadmap on Spin-Wave Computing. *arXiv e-prints*, page arXiv:2111.00365, October 2021.
- [8] Vladimir Cherepanov, Igor Kolokolov, and Victor L'vov. The saga of yig: Spectra, thermodynamics, interaction and relaxation of magnons in a complex magnet. *Physics Reports*, 229(3):81 – 144, 1993.
- [9] Iacopo Bertelli, Joris J. Carmiggelt, Tao Yu, Brecht G. Simon, Coosje C. Pothoven, Gerrit E. W. Bauer, Yaroslav M. Blanter, Jan Aarts, and Toeno van der Sar. Magnetic resonance imaging of spin-wave transport and interference in a magnetic insulator. *Science Advances*, 6(46):eabd3556, 2020.
- [10] Paolo Andrich, Charles F. de las Casas, Xiaoying Liu, Hope L. Bretscher, Jonson R. Berman, F. Joseph Heremans, Paul F. Nealey, and David D. Awschalom. Long-range spin wave mediated control of defect qubits in nanodiamonds. *npj Quantum Information*, 3(1):28, Jul 2017.
- [11] Ö. O. Soykal and M. E. Flatté. Strong field interactions between a nanomagnet and a photonic cavity. *Phys. Rev. Lett.*, 104:077202, Feb 2010.
- [12] Xufeng Zhang, Chang-Ling Zou, Liang Jiang, and Hong X. Tang. Strongly coupled magnons and cavity microwave photons. *Phys. Rev. Lett.*, 113:156401, Oct 2014.
- [13] Yutaka Tabuchi, Seiichiro Ishino, Toyofumi Ishikawa, Rekishu Yamazaki, Koji Usami, and Yasunobu Nakamura. Hybridizing ferromagnetic magnons and microwave photons in the quantum limit. *Phys. Rev. Lett.*, 113:083603, Aug 2014.
- [14] J. A. Haigh, A. Nunnenkamp, A. J. Ramsay, and A. J. Ferguson. Triple-resonant brillouin light scattering in magneto-optical cavities. *Phys. Rev. Lett.*, 117:133602, Sep 2016.
- [15] A. Osada, R. Hisatomi, A. Noguchi, Y. Tabuchi, R. Yamazaki, K. Usami, M. Sadgrove, R. Yalla, M. Nomura, and Y. Nakamura. Cavity optomagnonics with spin-orbit coupled photons. *Phys. Rev. Lett.*, 116:223601, Jun 2016.
- [16] Silvia Viola Kusminskiy, Hong X. Tang, and Florian Marquardt. Coupled spin-light dynamics in cavity optomagnonics. *Phys. Rev. A*, 94:033821, Sep 2016.
- [17] Xufeng Zhang, Na Zhu, Chang-Ling Zou, and Hong X. Tang. Optomagnonic whispering gallery microresonators. *Phys. Rev. Lett.*, 117:123605, Sep 2016.
- [18] J.A. Haigh, R.A. Chakalov, and A.J. Ramsay. Subpicoliter magnetooptical cavities. *Phys. Rev. Applied*, 14:044005, Oct 2020.
- [19] Jasmin Graf, Hannes Pfeifer, Florian Marquardt, and Silvia Viola Kusminskiy. Cavity optomagnonics with magnetic textures: Coupling a magnetic vortex to light. *Phys. Rev. B*, 98:241406, Dec 2018.
- [20] Jasmin Graf, Sanchar Sharma, Hans Huebl, and Silvia Viola Kusminskiy. Design of an optomagnonic crystal: Towards optimal magnon-photon mode matching at the microscale. *Phys. Rev. Research*, 3:013277, Mar 2021.
- [21] V. A. S. V. Bittencourt, I. Liberal, and S. Viola Kusminskiy. Optomagnonics in dispersive media: magnon-photon coupling enhancement at the epsilon-near-zero frequency. *arXiv e-prints*, October 2021.
- [22] Na Zhu, Xufeng Zhang, Xu Han, Chang-Ling Zou, Changchun Zhong, Chiao-Hsuan Wang, Liang Jiang, and Hong X. Tang. Waveguide cavity optomagnonics for microwave-to-optics conversion. *Optica*, 7(10):1291–1297, Oct 2020.

- [23] Sanchar Sharma, Babak Zare Rameshti, Yaroslav M. Blanter, and Gerrit E. W. Bauer. Optimal mode matching in cavity optomagnonics. *Phys. Rev. B*, 99:214423, Jun 2019.
- [24] Xufeng Zhang, Chang-Ling Zou, Liang Jiang, and Hong X. Tang. Cavity magnomechanics. *Science Advances*, 2(3), 2016.
- [25] Carlos Gonzalez-Ballester, Jan Gieseler, and Oriol Romero-Isart. Quantum acoustomechanics with a micromagnet. *Phys. Rev. Lett.*, 124:093602, Mar 2020.
- [26] Bret Heinrich, Yaroslav Tserkovnyak, Georg Woltersdorf, Arne Brataas, Radovan Urban, and Gerrit E. W. Bauer. Dynamic exchange coupling in magnetic bilayers. *Phys. Rev. Lett.*, 90:187601, May 2003.
- [27] Yi Li, Wei Cao, Vivek P. Amin, Zhizhi Zhang, Jonathan Gibbons, Joseph Sklenar, John Pearson, Paul M. Haney, Mark D. Stiles, William E. Bailey, Valentine Novosad, Axel Hoffmann, and Wei Zhang. Coherent spin pumping in a strongly coupled magnon-magnon hybrid system. *Phys. Rev. Lett.*, 124:117202, Mar 2020.
- [28] G. Woltersdorf, O. Mosendz, B. Heinrich, and C. H. Back. Magnetization dynamics due to pure spin currents in magnetic double layers. *Phys. Rev. Lett.*, 99:246603, Dec 2007.
- [29] Vittorio Giovannetti, Seth Lloyd, and Lorenzo Maccone. Quantum-Enhanced Measurements: Beating the Standard Quantum Limit. *Science*, 306(5700):1330–1336, November 2004.
- [30] Dany Lachance-Quirion, Yutaka Tabuchi, Seiichiro Ishino, Atsushi Noguchi, Toyofumi Ishikawa, Rekishu Yamazaki, and Yasunobu Nakamura. Resolving quanta of collective spin excitations in a millimeter-sized ferromagnet. *Science Advances*, 3(7):e1603150, July 2017.
- [31] Dany Lachance-Quirion, Samuel Piotr Wolski, Yutaka Tabuchi, Shingo Kono, Koji Usami, and Yasunobu Nakamura. Entanglement-based single-shot detection of a single magnon with a superconducting qubit. *Science*, 367(6476):425–428, January 2020.
- [32] Me. Dissipation-Based Quantum Sensing of Magnons with a Superconducting Qubit. *Physical Review Letters*, 125(11):117701, sep 2020.
- [33] Yutaka Tabuchi, Seiichiro Ishino, Atsushi Noguchi, Toyofumi Ishikawa, Rekishu Yamazaki, Koji Usami, and Yasunobu Nakamura. Coherent coupling between a ferromagnetic magnon and a superconducting qubit. *Science*, 349(6246):405–408, 2015.
- [34] Dany Lachance-Quirion, Yutaka Tabuchi, Arnaud Gloppe, Koji Usami, and Yasunobu Nakamura. Hybrid quantum systems based on magnonics. *Applied Physics Express*, 12(7):070101, jun 2019.
- [35] Babak Zare Rameshti, Silvia Viola Kusminskiy, James A. Haigh, Koji Usami, Dany Lachance-Quirion, Yasunobu Nakamura, Can-Ming Hu, Hong X. Tang, Gerrit E. W. Bauer, and Yaroslav M. Blanter. Cavity Magnonics. *arXiv e-prints*, page arXiv:2106.09312, June 2021.
- [36] Sanchar Sharma, Victor A. S. V. Bittencourt, Alexy D. Karenowska, and Silvia Viola Kusminskiy. Spin cat states in ferromagnetic insulators. *Phys. Rev. B*, 103:L100403, Mar 2021.
- [37] Victor A. S. V. Bittencourt, Verena Feulner, and Silvia Viola Kusminskiy. Magnon heralding in cavity optomagnonics. *Phys. Rev. A*, 100:013810, Jul 2019.
- [38] Feng-Xiao Sun, Sha-Sha Zheng, Yang Xiao, Qihuang Gong, Qiongyi He, and Ke Xia. Remote generation of magnon schrödinger cat state via magnon-photon entanglement. *Phys. Rev. Lett.*, 127:087203, Aug 2021.
- [39] Mehrdad Elyasi, Yaroslav M. Blanter, and Gerrit E. W. Bauer. Resources of nonlinear cavity magnonics for quantum information. *Physical Review B*, 101(5):054402, February 2020.
- [40] C. K. Law and J. H. Eberly. Arbitrary control of a quantum electromagnetic field. *Physical Review Letters*, 76(7):1055–1058, February 1996.
- [41] T. Holstein and H. Primakoff. Field dependence of the intrinsic domain magnetization of a ferromagnet. *Phys. Rev.*, 58:1098–1113, Dec 1940.
- [42] Daniel D. Stancil and Anil Prabhakar. *Spin waves: theory and applications*. Springer, New York, 2009. OCLC: ocn209335955.
- [43] Alexandre Blais, Ren-Shou Huang, Andreas Wallraff, S. M. Girvin, and R. J. Schoelkopf. Cavity quantum electrodynamics for superconducting electrical circuits: An architecture for quantum computation. *Physical Review A*, 69(6):062320, June 2004.

- [44] Alexandre Blais, Arne L. Grimsmo, S. M. Girvin, and Andreas Wallraff. Circuit quantum electrodynamics. *Rev. Mod. Phys.*, 93:025005, May 2021.
- [45] Jens Koch, Terri M. Yu, Jay Gambetta, A. A. Houck, D. I. Schuster, J. Majer, Alexandre Blais, M. H. Devoret, S. M. Girvin, and R. J. Schoelkopf. Charge-insensitive qubit design derived from the cooper pair box. *Phys. Rev. A*, 76:042319, Oct 2007.
- [46] P Krantz, M Kjaergaard, F Yan, T P Orlando, S Gustavsson, and W D Oliver. A quantum engineer’s guide to superconducting qubits. *Applied Physics Reviews*, page 58, 2019.
- [47] M. A. Rol, F. Battistel, F. K. Malinowski, C. C. Bultink, B. M. Tarasinski, R. Vollmer, N. Haider, N. Muthusubramanian, A. Bruno, B. M. Terhal, and L. DiCarlo. Fast, high-fidelity conditional-phase gate exploiting leakage interference in weakly anharmonic superconducting qubits. *Phys. Rev. Lett.*, 123:120502, Sep 2019.
- [48] Max Hofheinz, H. Wang, M. Ansmann, Radoslaw C. Bialczak, Erik Lucero, M. Neeley, A. D. O’Connell, D. Sank, J. Wenner, John M. Martinis, and A. N. Cleland. Synthesizing arbitrary quantum states in a superconducting resonator. *Nature*, 459(7246):546–549, May 2009.
- [49] M. D. Hutchings, J. B. Hertzberg, Y. Liu, N. T. Bronn, G. A. Keefe, Markus Brink, Jerry M. Chow, and B. L. T. Plourde. Tunable superconducting qubits with flux-independent coherence. *Phys. Rev. Applied*, 8:044003, Oct 2017.
- [50] Hugo Ribeiro, Alexandre Baksic, and Aashish A. Clerk. Systematic Magnus-Based Approach for Suppressing Leakage and Nonadiabatic Errors in Quantum Dynamics. *Physical Review X*, 7(1):011021, February 2017.
- [51] T. Figueiredo Roque, Aashish A. Clerk, and Hugo Ribeiro. Engineering fast high-fidelity quantum operations with constrained interactions. *npj Quantum Information*, 7(1):28, December 2021.
- [52] J.R. Johansson, P.D. Nation, and Franco Nori. Qutip: An open-source python framework for the dynamics of open quantum systems. *Computer Physics Communications*, 183(8):1760–1772, 2012.
- [53] J.R. Johansson, P.D. Nation, and Franco Nori. Qutip 2: A python framework for the dynamics of open quantum systems. *Computer Physics Communications*, 184(4):1234–1240, 2013.
- [54] H. Y. Yuan, W. P. Sterk, Akashdeep Kamra, and Rembert A. Duine. Pure dephasing of magnonic quantum states. *arXiv e-prints*, page arXiv:2201.06637, January 2022.
- [55] K. E. Cahill and R. J. Glauber. Ordered expansions in boson amplitude operators. *Phys. Rev.*, 177:1857–1881, Jan 1969.
- [56] K. E. Cahill and R. J. Glauber. Density operators and quasiprobability distributions. *Phys. Rev.*, 177:1882–1902, Jan 1969.
- [57] Nissim Ofek, Andrei Petrenko, Reinier Heeres, Philip Reinhold, Zaki Leghtas, Brian Vlastakis, Yehan Liu, Luigi Frunzio, S. M. Girvin, L. Jiang, Mazhar Mirrahimi, M. H. Devoret, and R. J. Schoelkopf. Extending the lifetime of a quantum bit with error correction in superconducting circuits. *Nature*, 536(7617):441–445, August 2016.
- [58] H. Jeong and M. S. Kim. Efficient quantum computation using coherent states. *Phys. Rev. A*, 65:042305, Mar 2002.
- [59] T. C. Ralph, A. Gilchrist, G. J. Milburn, W. J. Munro, and S. Glancy. Quantum computation with optical coherent states. *Phys. Rev. A*, 68:042319, Oct 2003.
- [60] Mazhar Mirrahimi, Zaki Leghtas, Victor V Albert, Steven Touzard, Robert J Schoelkopf, Liang Jiang, and Michel H Devoret. Dynamically protected cat-qubits: a new paradigm for universal quantum computation. *New Journal of Physics*, 16(4):045014, April 2014.
- [61] W. J. Munro, K. Nemoto, G. J. Milburn, and S. L. Braunstein. Weak-force detection with superposed coherent states. *Phys. Rev. A*, 66:023819, Aug 2002.
- [62] P. A. Knott, T. J. Proctor, A. J. Hayes, J. P. Cooling, and J. A. Dunningham. Practical quantum metrology with large precision gains in the low-photon-number regime. *Phys. Rev. A*, 93:033859, Mar 2016.
- [63] Jiahao Huang, Xizhou Qin, Honghua Zhong, Yongguan Ke, and Chaohong Lee. Quantum metrology with spin cat states under dissipation. *Scientific Reports*, 5(1):17894, Dec 2015.

- [64] T. C. Ralph. Coherent superposition states as quantum rulers. *Phys. Rev. A*, 65:042313, Apr 2002.
- [65] Roy J. Glauber. Coherent and incoherent states of the radiation field. *Phys. Rev.*, 131:2766–2788, Sep 1963.
- [66] <https://github.com/sancharsharma/Magnon-State-Generation>.
- [67] F. Motzoi, J. M. Gambetta, P. Rebentrost, and F. K. Wilhelm. Simple pulses for elimination of leakage in weakly nonlinear qubits. *Phys. Rev. Lett.*, 103:110501, Sep 2009.
- [68] Zijun Chen, Julian Kelly, Chris Quintana, R. Barends, B. Campbell, Yu Chen, B. Chiaro, A. Dunsworth, A. G. Fowler, E. Lucero, E. Jeffrey, A. Megrant, J. Mutus, M. Neeley, C. Neill, P. J. J. O’Malley, P. Roushan, D. Sank, A. Vainsencher, J. Wenner, T. C. White, A. N. Korotkov, and John M. Martinis. Measuring and suppressing quantum state leakage in a superconducting qubit. *Phys. Rev. Lett.*, 116:020501, Jan 2016.
- [69] Sahel Ashhab, Fumiki Yoshihara, Tomoko Fuse, Naoki Yamamoto, Adrian Lupascu, and Kouichi Semba. Speed limits for quantum gates with weakly anharmonic qubits. *arXiv e-prints*, September 2021.
- [70] M. Werninghaus, D. J. Egger, F. Roy, S. Machnes, F. K. Wilhelm, and S. Filipp. Leakage reduction in fast superconducting qubit gates via optimal control. *npj Quantum Information*, 7(1):14, December 2021.
- [71] Shabnam Safaei, Simone Montangero, Fabio Taddei, and Rosario Fazio. Optimized single-qubit gates for josephson phase qubits. *Phys. Rev. B*, 79:064524, Feb 2009.
- [72] P. Rebentrost and F. K. Wilhelm. Optimal control of a leaking qubit. *Phys. Rev. B*, 79:060507, Feb 2009.
- [73] Katharina Rojan, Daniel M. Reich, Igor Dotsenko, Jean-Michel Raimond, Christiane P. Koch, and Giovanna Morigi. Arbitrary-quantum-state preparation of a harmonic oscillator via optimal control. *Phys. Rev. A*, 90:023824, Aug 2014.
- [74] Nicolas Wittler, Federico Roy, Kevin Pack, Max Werninghaus, Anurag Saha Roy, Daniel J. Egger, Stefan Filipp, Frank K. Wilhelm, and Shai Machnes. Integrated tool set for control, calibration, and characterization of quantum devices applied to superconducting qubits. *Phys. Rev. Applied*, 15:034080, Mar 2021.
- [75] Sergey Bravyi, David P. DiVincenzo, and Daniel Loss. Schrieffer–wolff transformation for quantum many-body systems. *Annals of Physics*, 326(10):2793–2826, 2011.